REPORT DOCUMENTATION PAGE

Form Approved
OMB No. 0704-0188

1. REPORT DATE *(DD-MM-YYYY)*	**2. REPORT TYPE**	**3. DATES COVERED** *(From - To)*
September 2013	Journal Article	September 2013- June 2014

4. TITLE AND SUBTITLE
Complexity Reduction of Collisional-Radiative Kinetics for Atomic Plasma

5a. CONTRACT NUMBER
In-House

5b. GRANT NUMBER

5c. PROGRAM ELEMENT NUMBER

6. AUTHOR(S)
Hai Le, Jean-Luc Cambier and Ann Karagozian

5d. PROJECT NUMBER

5e. TASK NUMBER

5f. WORK UNIT NUMBER
Q0AE

7. PERFORMING ORGANIZATION NAME(S) AND ADDRESS(ES)

Air Force Research Laboratory (AFMC)
AFRL/RQRS
1 Ara Drive.
Edwards AFB, CA, 93524-7013

8. PERFORMING ORGANIZATION REPORT NO.

9. SPONSORING / MONITORING AGENCY NAME(S) AND ADDRESS(ES)

Air Force Research Laboratory (AFMC)
AFRL/RQR
5 Pollux Dr.
Edwards AFB, CA, 93524-7048

10. SPONSOR/MONITOR'S ACRONYM(S)

11. SPONSOR/MONITOR'S REPORT NUMBER(S)
AFRL-RQ-ED-JA-2013-242

12. DISTRIBUTION / AVAILABILITY STATEMENT
Approved for public release; distribution unlimited

13. SUPPLEMENTARY NOTES
Journal article published in the Physics of Plasmas, Vol. 20, December 2013.
PA Case Number: 13502; Clearance Date: 18 Oct 13.

14. ABSTRACT
Thermal non-equilibrium processes in partially ionized plasmas can be most accurately modeled by collisional-radiative kinetics. This level of detail is required for an accurate prediction of the plasma. However, the resultant system of equations can be prohibitively large, making multidimensional and unsteady simulations of non-equilibrium radiating plasma particularly challenging. In this paper, we present a scheme for model reduction of the collisional-radiative kinetics, by combining energy levels into groups and deriving the corresponding macroscopic rates for all transitions. Although level-grouping is a standard approach to this type of problem, we provide here a mechanism for achieving higher-order accuracy by accounting for the level distribution within a group. The accuracy and benefits of the scheme are demonstrated for the generic case of atomic hydrogen by comparison with the complete solution of the master rate equations and other methods.

15. SUBJECT TERMS

16. SECURITY CLASSIFICATION OF:			**17. LIMITATION OF ABSTRACT**	**18. NUMBER OF PAGES**	**19a. NAME OF RESPONSIBLE PERSON**
c. REPORT	**b. ABSTRACT**	**c. THIS PAGE**			Jean-Luc Cambier
Unclassified	**Unclassified**	**Unclassified**	SAR	19	**19b. TELEPHONE NO** *(include area code)* 661-525-5655

Standard Form 298 (Rev. 8-98)
Prescribed by ANSI Std. 239.18

Complexity reduction of collisional-radiative kinetics for atomic plasma

Hai P. Le,[1,a)] Ann R. Karagozian,[2] and Jean-Luc Cambier[3,b)]
[1]*ERC Inc., Edwards AFB, California 93524, USA*
[2]*Department of Mechanical and Aerospace Engineering, University of California, Los Angeles, California 90095, USA*
[3]*Air Force Research Laboratory, Edwards AFB, California 93524, USA*

(Received 9 October 2013; accepted 3 December 2013; published online 23 December 2013)

Thermal non-equilibrium processes in partially ionized plasmas can be most accurately modeled by collisional-radiative kinetics. This level of detail is required for an accurate prediction of the plasma. However, the resultant system of equations can be prohibitively large, making multi-dimensional and unsteady simulations of non-equilibrium radiating plasma particularly challenging. In this paper, we present a scheme for model reduction of the collisional-radiative kinetics, by combining energy levels into groups and deriving the corresponding macroscopic rates for all transitions. Although level-grouping is a standard approach to this type of problem, we provide here a mechanism for achieving higher-order accuracy by accounting for the level distribution within a group. The accuracy and benefits of the scheme are demonstrated for the generic case of atomic hydrogen by comparison with the complete solution of the master rate equations and other methods. © *2013 AIP Publishing LLC*. [http://dx.doi.org/10.1063/1.4849417]

I. INTRODUCTION

The ability to model plasma flows with non-equilibrium chemistry plays an important role in a number of applications including but not limited to plasma propulsion,[1] high-speed reentry flows,[2] plasma-assisted combustion and interpretation of laser diagnostics.[3] In order to better understand the physical characteristics of the flow and the coupling with chemistry under the conditions of interests, one needs to accurately model all the non-equilibrium processes associated with the atoms and molecules (e.g., excitation, ionization, and dissociation) through collisional and radiative interactions.[4–6] The most accurate treatment for these non-equilibrium plasmas requires a state-to-state approach,[7–13] also referred to as collisional-radiative (CR) models, in which deviations from the equilibrium distribution of the internal states can be captured.

These CR models, although very accurate from a physics point of view, can be computationally very expensive due to the large number of internal states for which the number densities must be computed. For an atomic plasma, these states correspond to all the electronic excitation levels of the various neutral and ion species considered. For a molecular plasma, additional degrees of freedom such as the rotational and vibrational modes further increase the level of complexity. In addition, these molecular degrees of freedom are strongly coupled to the chemical reactions. For example, vibrational excitation facilitates dissociation or other endothermic reactions, and recombination can also favor the production of excited states. These models, derived from *ab initio* cross section databases for all elementary processes, can be applied to a wide range of plasma conditions and offer more complete insight into the non-equilibrium effects. For example, a recent study of ionizing shocks in Argon by Kapper and Cambier[10,11] demonstrated that this level of detail is needed for an accurate prediction of high-speed flows. In addition, the unsteady coupling of the hydrodynamics and CR kinetics leads to physical phenomena which can, in turn, provide additional information useful for model validation and/or experimental measurements of various parameters.

Due to the large computational workload involved in solving the CR master equations, simulations incorporating state-to-state kinetics have only been limited to zero- or one-dimension with a few exceptions of two-dimensional calculations.[11,14,15] For example, the run-time for solving a set of rate equations for the CR kinetics of atomic hydrogen scales as the cubic power of the size of the atomic state distribution function (ASDF) when an implicit, backward-Euler method is employed. While better scaling laws could be obtained with iterative and more approximate schemes, their accuracy and stability for extremely stiff problems are still an issue. The development of very efficient and accurate schemes for CR kinetics is still an ongoing research topic which will be presented elsewhere; here, we discuss a different approach, consisting of lowering the complexity of the calculations by developing a reduced-order kinetic model suitable for multi-dimensional flow calculations while maintaining a sufficient level of detail required to accurately model the plasma. Several mechanism reduction schemes have been proposed in the literature with applications to various types of kinetics. Colonna *et al.*[16] utilize a two-level distribution model to study nitrogen dissociation rates in recombining flows, in which all the vibrational levels except for the last level are modeled by a single energy equation with an assumption of a Boltzmann distribution, and the last vibrational level is modeled using state-to-state kinetics to take in account the non-equilibrium effects of the upper states. Magin *et al.*[17] have

[a)]Also at Department of Mechanical and Aerospace Engineering, University of California, Los Angeles, California 90095, USA.
[b)]Author to whom correspondence should be addressed. Electronic mail: jean_luc.cambier@us.af.mil

developed a rovibrational collisional (RVC) coarse-grain model to characterize the internal energy excitation and dissociation processes of nitrogen flow behind a strong shock wave. The coarse-grain model is derived by lumping the rovibrational energy levels into groups, in which the population is described by a uniform distribution. Guy *et al.*[18] proposed a multi-internal-temperatures models for a vibrationally non-equilibrium flow, in which the vibrational distribution is divided into two or three groups, each with its own vibrational temperature. Liu *et al.*,[19] on the other hand, proposed a mechanism reduction to CR models based on the multi-group maximum entropy principle with the constraints being the macroscopic parameters.

In this paper, we examine several different level grouping schemes for the state-to-state kinetics of *atomic* electronic states. The first approach is similar to that of Magin *et al.*[17] for the rovibrational collisional coarse-grain model and therefore is based on uniform (U) binning of the levels. The second approach here consists of grouping levels into groups with an assumed Boltzmann (B) distribution, allowing a higher-order description of the ASDF. In this case, the effective excitation temperatures are evolved in time by conserving a set of moments of the distribution function; the most obvious solution is to solve for number density and energy, similar to the approach by Guys *et al.*[18] However, we will show that a different set of moment variables of the same order should be used, due to the specific nature of the ASDF.

The method developed here can be applied to a wide range of state-to-state kinetics models including the RVC[13,17] and vibrational[9] collisional (VC) models or the electronic collisional-radiative model.[8,10–12,20] In the interest of simplicity, we consider here the CR model of atomic hydrogen, using classical models for the level energies and rates; the actual values of these parameters are unimportant here, as long as the structure of the ASDF is representative of the actual species, notably the geometric progression of the level energies of the ASDF and the stiffness ratio. The level grouping techniques are applied to reduce the cost of solving the full master equations and the results are compared with the reference solution computed from the full master equations.

The rest of the paper is organized as follows: we describe the state-to-state kinetics and numerical solution in Sec. II, while in Sec. III we describe the various mechanism reduction methods. We compare the results of the reduced-order models with the full set of master equations in Sec. IV and examine the issue of energy conservation in Sec. V. Finally, a summary is given in Sec. VI, while the derivation of the kinetic rates used in this study is given in Appendix.

II. COLLISIONAL-RADIATIVE MODEL

A. Definitions and rates

As mentioned above, we consider here the ASDF of atomic hydrogen coupled to electron impact excitation and ionization, and the reverse processes (respectively, deexcitation and recombination), as well as the radiative rates for line transitions in an optically thin approximation. Radiative recombination is neglected and all radiation absorption is ignored, as is free-free (Bremsstrahlung) emission, since this does not directly affect the atomic level populations.[21] The atomic states of the hydrogen atom are listed as a function of their principal quantum number (n) only, following the Bohr atomic model; the splitting of states with respect to orbital and spin numbers is ignored, and all states have a degeneracy $g_n = 2n^2$. The states number from $n = 1$ to ∞ and we consider a finite number of states $n = 1, \ldots, M < \infty$ before reaching the ionization limit.[22] In this simplified model, the energy of each state is given as $E_n = I_H\left(1 - 1/n^2\right)$, as measured from the ground state ($E_1 \equiv 0$), and we will denote by $I_n = I_H\left(1/n^2 - 1/M^2\right) \simeq I_H/n^2$ the energy required for ionization of level n.

The population density N_n is the number of atoms per unit volume of a state n. For a single bound-bound transition between states n and m ($m > n$) induced by electron-impact collisions, the rate of change of the population density is of the form

$$\frac{dN_n}{dt} = -\alpha^e_{(m|n)} N_n N_e + \beta^e_{(n|m)} N_m N_e. \tag{1}$$

Hereafter, we will use the convention of indexing the rates with the final state on the left, and the initial state on the right, i.e., $(f|i)$. The first term on the right of Eq. (1) describes the loss due to excitation from level n to m, as a result of collisions between free electrons (of number density N_e); the second term describes the gain due to collisional deexcitation from the state m, with number density N_m. Note that for the same transition between the levels n and m, we also have

$$\frac{dN_m}{dt} = +\alpha^e_{(m|n)} N_n N_e - \beta^e_{(n|m)} N_m N_e. \tag{2}$$

If there were only two states to consider, Eq. (1) would be the entire rate of change for level n, but since all transitions involving the state n must be counted, the rate of change for excitation and deexcitation alone involves summing up the right hand side over all levels $m \neq n$. At equilibrium (Boltzmann), the ratio of population densities is

$$\frac{N^*_m}{N^*_n} \equiv \mathcal{B}_{nm}(T_e) = \frac{g_m}{g_n} e^{-\Delta E_{nm}/kT_e}, \tag{3}$$

where $\Delta E_{nm} = E_m - E_n$ is the difference in level energies. For electron-impact processes, the rates α and β in Eqs. (1) and (2) are functions of T_e and are given by Eqs. (A9a) and (A9b) in Appendix. For low values of the energy gaps between levels ($\Delta E_{nm}/kT \ll 1$), both forward (α) and backward (β) rates become very large. This leads to a wide range of time scales as the number of levels is increased, and to a considerable stiffness in the system of equations. For example, Figure 1 demonstrates the increase in both the maximum eigenvalue (inverse time scale) and the spread of values, i.e., stiffness, as the plasma evolves as function of time. Additionally, Eqs. (A9a) and (A9b) show that the system is strongly diagonally dominant, in the sense that transitions with small changes in quantum number ($m - n \simeq 1$) have a

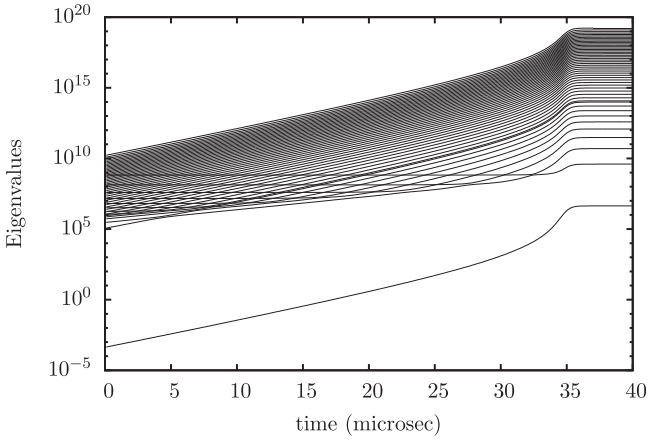

FIG. 1. Spectrum of eigenvalues of the CR system versus time, during constant-T_e plasma evolution from a low-temperature ASDF and low electron number density; as excitation and ionization proceed, the upper states and N_e increase, yielding a rapid growth of the characteristic frequencies.

higher rate than those with $m - n \gg 1$. In fact, a fairly good approximation here could be to consider a ladder process, i.e., transitions between neighboring states only, but this is not necessarily applicable to other atomic configurations, and this approximation is not used here.

For ionization and recombination processes, the rate of change of the population density for level n is

$$\frac{dN_n}{dt} = -\alpha^e_{(+|n)} N_n N_e + \beta^e_{(n|+)} N_+ N_e^2. \tag{4}$$

The first term on the right side is the loss due to ionization of that level by electron collisions (N_e), while the second term is due to the capture by an ion (N_+) of a free electron (one factor of N_e), in the presence of a second electron (leading to an N_e^2 dependence), required for energy conservation. The equilibrium for ionization and recombination (Saha) involves a different relation

$$\left(\frac{N_+ N_e}{N_n}\right)^* \equiv \mathcal{S}_n(T_e) = \frac{g_+}{g_n} 2 \left(\frac{2\pi m_e k T_e}{h^2}\right)^{3/2} e^{-I_n/kT_e}, \tag{5}$$

where g_+ is the degeneracy of the ion ground state (for atomic hydrogen, $g_+ \equiv 1$). Thus, we cannot assume that the equilibrium values are the same for both excitation/deexcitation and ionization/recombination processes. Usually, we can have Boltzmann equilibrium (3) without Saha equilibrium, but hardly the reverse, mostly because it takes more energy to ionize than to excite; for the upper states close to the ionization limit ($n \gg 1$), the difference is less significant.

Only the radiative transitions between atomic levels ("line," or "bound-bound" emission) are considered here. For each bound-bound transition $m \to n$ ($m > n$), we have

$$\frac{dN_n}{dt} = +A_{(n|m)} N_m, \tag{6}$$

$$\frac{dN_m}{dt} = -A_{(n|m)} N_m. \tag{7}$$

B. Master equations

Once all the macroscopic rates are obtained, we can construct the master equations describing the collisional-radiative kinetics of all levels. In this study, we consider atomic hydrogen, which has only one ion state, and only electron collisions, which allows us to remove the superscript e in the rate definition hereafter. The rate of change of the population density of a level n is thus written as

$$\begin{aligned}\frac{dN_n}{dt} = &-\sum_{m>n} \alpha_{(m|n)} N_e N_n + \sum_{m>n} \beta_{(n|m)} N_e N_m + \sum_{m>n} A_{(n|m)} N_m \\ &+ \sum_{m<n} \alpha_{(n|m)} N_e N_m - \sum_{m<n} \beta_{(m|n)} N_e N_n - \sum_{m<n} A_{(m|n)} N_n \\ &- \alpha_{(+|n)} N_e N_n + \beta_{(n|+)} N_+ N_e^2. \end{aligned} \tag{8}$$

Similarly, we can write another equation for the rate of change of the population density of the ions according to the rate of ionization or recombination

$$\frac{dN_+}{dt} = \sum_n \alpha_{(+|n)} N_e N_n - \sum_n \beta_{(n|+)} N_+ N_e^2. \tag{9}$$

Finally, the electron density is related to the ion density by the charge neutrality condition

$$N_e = \sum_q Z_q N_q. \tag{10}$$

We will compute the time evolution of a uniform plasma; if we assume a constant temperature bath, the conservation equations above constitute a complete set, but for constant-volume conditions—with time variation of the temperature—there is also conservation equation for the electron energy, which will be examined in more detail in Sec. V. The task of deriving a reduced model for the CR kinetics aims at modeling the shape of the ASDF at a lower computational cost compared to that required to solve the full master equations, while maintaining sufficient accuracy to capture the non-equilibrium effects. The most natural way to accomplish this is to partition the excited states into groups or "bins," therefore reducing the number of variables in the system. Various assumptions can be made about the internal structure of each group, i.e., the distribution of states *within* the groups, and various approaches to solving the group-based variables can be devised.

C. Numerical solution

Examination of Eqs. (8) and (9) reveals that the full system of ODEs can be written in the following form:

$$\frac{dX_p}{dt} = -\mathbf{J}_p \cdot X_p + \sum_q \mathbf{K}_{pq} X_q \quad \{p,q\} \in \{1,\ldots,M,1^+\}, \tag{11}$$

where X_p is the p-element of the vector of conserved variables—for the set of master equations (8), $X_p \equiv N_p$—and $\mathbf{J}_p$, $\mathbf{K}_{pq}$ are matrices built from summation over all possible transitions between levels, and are themselves functions of

X_p. Thus, the source term can generally be decomposed into a linear and non-linear terms. The system (11) can be solved using a variety of techniques. In this study, we have used a backward Euler scheme to avoid the stiffness of the CR kinetics. Expanding the general system (11)

$$dX_p = -(\mathbf{J}_p + d\mathbf{J}_p)\cdot(X_p + dX_p) + \sum_q (\mathbf{K}_{pq} + d\mathbf{K}_{pq})(X_q + dX_q) \tag{12}$$

and retaining 1st-order terms only, we obtain

$$\mathbf{A}_{pr}\cdot dX_r \simeq -\mathbf{J}_p\cdot X_p + \sum_q \mathbf{K}_{pq}\cdot X_q \tag{13}$$

with the Jacobian

$$\mathbf{A}_{pr} = (1+\mathbf{J}_p)\delta_{pr} - \mathbf{K}_{pr} + X_p\left(\frac{\partial \mathbf{J}_p}{\partial X_r}\right) - \sum_q X_q\left(\frac{\partial \mathbf{K}_{pq}}{\partial X_r}\right). \tag{14}$$

For this implicit method, there is no stability restriction on the time step. For consistency, all the simulations shown in this paper utilized a constant time step. The same solution methodology is applied to the various cases of level groupings, where now some of the conserved variables in the set $\{X_p\}$ are summations over the levels within the groups/bins, while in the general case of non-isothermal plasma, it also includes the electron energy E_e.

III. LEVEL GROUPING STRATEGIES

A. Uniform grouping

Consider a group of M individual levels $i = \{n_0, \ldots, n_{M-1}\}$, abbreviated as $i \in n$ and denote the group, or "bin" number by n; hereafter, n, m,… are the group indices and i, j,… are level indices. This first approach to model reduction is essentially a zeroth-order approximation of the internal[23] distribution function, where only one moment variable, either the total number density of the group or the total excitation energy of the group, is required. The traditional choice is to conserve the total number density of the group, i.e., $\mathcal{N}_n = \sum_{i\in n} N_i$. Using Eq. (3), a Boltzmann approximation of the internal partition function $\mathcal{Z}_n$ is obtained by[24]

$$\mathcal{N}_n = N_{n_0}\sum_{i\in n}\frac{N_i}{N_{n_0}} \simeq \frac{N_{n_0}}{g_{n_0}}\underbrace{\sum_{i\in n} g_i e^{-\Delta E_i/T_n}}_{\mathcal{Z}_n}, \tag{15}$$

where $\Delta E_i = E_i - E_{n_0}$ is the difference in energy between the level i and the first level of the group, n_0. The approximation of a group with uniform internal distribution is equivalent to having a characteristic group temperature T_n approaching infinity, compared to the total energy width of the group, i.e.,

$$\mathcal{Z}_n \to g_n = \sum_{i\in n} g_i, \tag{16}$$

where g_n is the overall group degeneracy. The simplest model therefore consists of assuming all levels within the group to be distributed uniformly, i.e., weighted by the level degeneracy

$$N_i = \frac{g_i}{g_n}\mathcal{N}_n. \tag{17}$$

The rate equation for a group n is obtained by summing the master rate equations (8) and (9) for all the levels i within the group, and utilizing relation (15)

$$\begin{aligned}\frac{d\mathcal{N}_n}{dt} =& -N_e\mathcal{N}_n\left[\sum_{m>n}\sum_{i\in n}\frac{g_i}{g_n}\sum_{j\in m}\alpha_{(j|i)} + \sum_{m<n}\sum_{i\in n}\frac{g_i}{g_n}\sum_{j\in m}\beta_{(j|i)}\right]\\ &+N_e\mathcal{N}_m\left[\sum_{m<n}\sum_{i\in n}\sum_{j\in m}\frac{g_j}{g_m}\alpha_{(i|j)} + \sum_{m>n}\sum_{i\in n}\sum_{j\in m}\frac{g_j}{g_m}\beta_{(i|j)}\right]\\ &-\mathcal{N}_n\left[\sum_{m<n}\sum_{i\in n}\frac{g_i}{g_n}\sum_{j\in m}A_{(j|i)}\right] + \mathcal{N}_m\left[\sum_{m>n}\sum_{i\in n}\sum_{j\in m}\frac{g_j}{g_m}A_{(i|j)}\right]\\ &-N_e\mathcal{N}_n\left[\sum_{i\in n}\frac{g_i}{g_n}\alpha_{(+|i)}\right] + N_e^2 N_+\left[\sum_{i\in n}\beta_{(i|+)}\right].\end{aligned} \tag{18}$$

Similarly for the ion state, one obtains

$$\frac{dN_+}{dt} = N_e\sum_n \mathcal{N}_n\left[\sum_{i\in n}\frac{g_i}{g_n}\alpha_{(+|i)}\right] - N_e^2 N_+\sum_n\left[\sum_{i\in n}\beta_{(i|+)}\right]. \tag{19}$$

The terms within brackets in Eqs. (18) and (19) contain *effective* rates for the groups, which can be pre-computed. For example, in the first term on the right-hand-side of Eq. (18)

$$\tilde{\alpha}_{(m|n)} = \sum_{i\in n}\frac{g_i}{g_n}\sum_{j\in m}\alpha_{(j|i)}$$

is an effective excitation rate from group n to group m. Note that since this model does not require computing an excitation temperature T_n, all the effective transition rates between the groups can be expressed as a function of the kinetic temperature T_e only. It is important to emphasize that the grouping of levels is applied on the high energy states only; thus in any simulation we must choose a number of low-energy, "resolved" levels, as well as a variable number of groups combining the upper states. The number of discrete states, the number of groups and their widths are variable parameters of the model, whether we use uniform binning as above, or Boltzmann internal distributions, discussed below. In order to bound this parameter space (optimization is beyond the scope of the present work), we need to provide a reference solution, such that the population density of each level can be compared to the one reconstructed from the assumed internal distribution within each group. Figure 2 shows the evolution of the electron density computed from the master equations. This test corresponds to a strong ionization regime

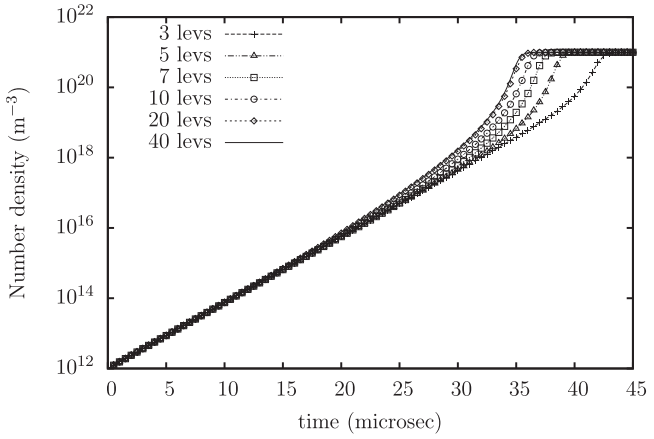

FIG. 2. Time evolution of the electron number density using different total number of atomic levels. The electron temperature is set at 3.0 eV.

and the time evolution of the ASDF shows an increasing population of the higher atomic levels while the electron density grows exponentially. It also demonstrates the effect of the number of levels included in the simulation, i.e., using a fewer number of atomic states has an impact on delaying the onset of the electron avalanche. This indicates that ionization from the high-energy states is an important process, and therefore the evolution of the upper states must be accurately captured. We could always increase the size of the ASDF to obtain higher accuracy, but with diminishing return; ultimately, the time-resolution of interest and the accuracy threshold dictate the number of levels required in a simulation. The mapping between the practical requirements and ASDF size is not a straightforward matter, but is an issue beyond the scope of this work. Convergence studies with respect to the size of the system showed that beyond 20 levels, there were no discernible differences in the results—see Figure 2. Thus, we chose our reference solution to be the one obtained for 20 levels, and all level-grouping models investigated here will be based on this extent of the ASDF.

B. Boltzmann grouping—Number and energy

Several assumptions can be made regarding a Boltzmann-like structure within the group. Panesi *et al.*[12] and Magin *et al.*[25] rely on the assumption that the population within a group follows a Boltzmann distribution at the kinetic temperature, i.e., in this case, $T_n \equiv T_e$. This approach is only valid if the rates of exchange between the levels within the group are much faster than the exchange rates with levels outside the group; otherwise, one could then assume that the entire ASDF is governed by T_e and is always in Boltzmann equilibrium. The validity of this assumption is highly questionable for atomic state populations.[26] Furthermore, when different collision partners must be considered, the kinetic temperature can be either that of the heavy particles or the electrons (e.g., electron-impact excitation and heavy impact quenching); in this case, choosing either one of the kinetic temperature can impact on the results.

In order to accurately describe the population of a group with a Boltzmann distribution, two moment variables of the ASDF need to be conserved. The selection of these variables, however, can be arbitrary. Guy *et al.*[18] conserved the total number density of the group and the average excitation energy; these, respectively, correspond to zeroth- and first-order moment variables, and would appear to be a natural choice. Consider the total number of states $\mathcal{N}_n$—defined in Eq. (15)—and the total energy within the bin $\mathcal{E}_n = \sum_{i\in n} E_i N_i$, for which we can write conservation equations, derived from Eq. (8)

$$\frac{d\mathcal{N}_n}{dt} = -N_e \mathcal{N}_n \left[\sum_{m>n} \sum_{i\in n} \frac{g_i e^{-\Delta E_i/T_n}}{\mathcal{Z}_n} \sum_{j\in m} \alpha_{(j|i)} + \sum_{m<n} \sum_{i\in n} \frac{g_i e^{-\Delta E_i/T_n}}{\mathcal{Z}_n} \sum_{j\in m} \beta_{(j|i)} \right] \ldots \tag{20a}$$

$$\frac{d\mathcal{E}_n}{dt} = -N_e \mathcal{N}_n \left[\sum_{m>n} \sum_{i\in n} \frac{g_i e^{-\Delta E_i/T_n}}{\mathcal{Z}_n} \sum_{j\in m} E_i \alpha_{(j|i)} + \sum_{m<n} \sum_{i\in n} \frac{g_i e^{-\Delta E_i/T_n}}{Z_n} \sum_{j\in m} E_i \beta_{(j|i)} \right] \ldots \tag{20b}$$

For sake of brevity, we did not write the entire list of contributions in Eq. (20), which can be easily derived from Eq. (18) by generalizing the weighting factors g_i/g_n to $g_i e^{-\Delta E_i/T_n}/\mathcal{Z}_n$, and similarly for other groups. By solving for total number and total energy of each group, according to Eqs. (20a) and (20b), we can guarantee direct conservation of both mass (total number of levels $\mathcal{N}_n$) and energy ($\mathcal{E}_n$). However, this approach presents some problems in determining the internal Boltzmann temperature, as will now be shown. First, let us define a total group/bin energy measured from the lower bound, i.e., $\Delta\mathcal{E}_n = \sum_{i\in n}(E_i - E_{n_0})N_i$; the rate of change of this shifted energy is still given by the right-hand-side of Eq. (20b). We can then write

$$\Delta\mathcal{E}_n = \frac{N_{n_0}}{g_{n_0}} \sum_{i\in n} g_i \, \Delta E_i \, e^{-\Delta E_i/T_n} = \mathcal{N}_n \langle \Delta E \rangle_n, \tag{21}$$

where

$$\langle \Delta E \rangle_n = \frac{1}{\mathcal{Z}_n} \sum_{i\in n} g_i \, \Delta E_i \, e^{-\Delta E_i/T_n} = T_n^2 \frac{d}{dT_n} \ln(\mathcal{Z}_n) \tag{22}$$

is the average group energy measured from the first internal level. Similarly, a specific heat at constant-volume can be determined, i.e.,

$$C_v(T_n) = \frac{d}{dT_n} \langle \Delta E \rangle_n = T_n^{-2} \left[\frac{\sum_{i\in n} g_i (\Delta E_i)^2 e^{-\Delta E_i/T_n}}{\mathcal{Z}_n} - \langle \Delta E \rangle_n^2 \right] = T_n^{-2} \left[\langle \Delta E^2 \rangle_n - \langle \Delta E \rangle_n^2 \right]. \tag{23}$$

Since $\mathcal{N}_n$ and $\mathcal{E}_n$ are conserved variables, we obtain new values at each time level (k) and in order to compute the Boltzmann temperature T_n, we need to iterate the equation

$$\langle \Delta E \rangle_n (T_n^*) + C_v(T_n^*)\delta T_n^* = \frac{\Delta \mathcal{E}_n^{(k)}}{\mathcal{N}_n^{(k)}}, \tag{24}$$

where T_n^* is the running iterated value, until convergence ($\delta T_n^* \simeq 0$). However, the slope of the curve $\langle \Delta E \rangle_n (T_n)$ is extremely flat at low temperature, i.e., $C_v \to 0$. In fact, when $T_n \to 0$, to the leading order we have: $\mathcal{N}_n \simeq N_{n_0} o(1+\epsilon)$, $\langle \Delta E \rangle_n \simeq o(\epsilon)$ and $C_v(T_n) \simeq o(\epsilon)$, where $\epsilon = e^{-\Delta E_1/T_n}$ is a small parameter. Therefore, during the iterations $\delta T_n^* = o(\epsilon)/o(\epsilon)$ and arbitrary temperature solutions can be obtained. Our studies showed that indeed, numerical instabilities prevent us from obtaining satisfactory solutions in many test cases. While it is possible to introduce limiters to prevent unphysical or improbable values and stop the iteration counters, this is not a satisfactory solution to the problem. We should also emphasize that the problem occurs when T_n is small, which does *not* imply that electronic levels are unpopulated, since we may very well have small *internal* group temperatures as a result of initial conditions or running iterations, but non-negligible overall electronic excitation ($\mathcal{N}_n \neq 0$).[27]

C. Boltzmann grouping—Partitioning

In the approach above, we are dealing with two reduced variables $\mathcal{N}_n$ and $\mathcal{E}_n$ (or $\Delta\mathcal{E}_n$) which are both summations over the internal levels. An alternative may consist of keeping one of the level populations as a variable. Therefore, we could instead choose for each group n to conserve the population of the lowest level in that group N_{n_0} and $\mathcal{N}_n$, whose evolution is given by a form similar to Eq. (20a). To evaluate the Boltzmann temperature of the group, we now have at time step (k), from Eq. (15):

$$\mathcal{N}_n^{(k)} = \frac{N_{n_0}^{(k)}}{g_{n_0}} \sum_{i \in n} g_i e^{-\Delta E_i/T_n} = \frac{N_{n_0}^{(k)}}{g_{n_0}} \mathcal{Z}_n(T_n^{(k)})$$

so that in order to evaluate the new bin temperature $T_n^{(k)}$ we need to solve

$$\mathcal{Z}_n(T_n^*) + \left(\frac{d\mathcal{Z}_n}{dT_n}\right)\delta T_n^* = \frac{\mathcal{N}_n^{(k)}}{N_{n_0}^{(k)}} g_{n_0} \tag{25}$$

until convergence. Using Eq. (22), this leads to

$$\delta T_n^* \simeq \frac{T_n^{*2}}{\mathcal{Z}_n(T_n^*)\langle \Delta E \rangle_n (T_n^*)} \left[\frac{\mathcal{N}_n^{(k)}}{N_{n_0}^{(k)}} g_{n_0} - \mathcal{Z}_n(T_n^*)\right], \tag{26}$$

where, again, the dependencies on temperature have been explicitly written. At low T_n, the denominator is $o(\epsilon)(1+\epsilon)$ and the numerator is a difference between two terms of $o(1+\epsilon)$. Therefore, the iterative procedure is again numerically unstable.

To attempt to alleviate this problem, we have examined yet another approach: for each group n we conserve the population of the lowest level in that group N_{n_0} and $\mathcal{N}'_n$, the total population of the *remaining* upper states n' of that group, such that $n = n_0 \cup n'$. This is an effective partitioning *within* the group, which allows us to separate the variables, one of $o(1)$ and the other of $o(\epsilon)$. Clearly, we have now

$$\mathcal{N}'_n = \frac{N_{n_0}}{g_{n_0}} \underbrace{\sum_{i \in n'} g_i e^{-\Delta E_i/T_n}}_{\mathcal{Z}'_n} \quad \text{using} \quad N_i = \frac{\mathcal{N}'_n}{\mathcal{Z}'_n} g_i e^{-\Delta E_i/T_n}. \tag{27}$$

In order to evaluate the new temperature from the two conserved variables, we iterate on δT_n^* using a form similar to Eq. (25)

$$\mathcal{Z}'_n(T_n^*) + \left(\frac{d\mathcal{Z}'_n}{dT_n}\right)\delta T_n^* = \frac{\mathcal{N}'^{(k)}_n}{N_{n_0}^{(k)}} g_{n_0}. \tag{28}$$

However, it is easy to see that since $\frac{d}{dT}\mathcal{Z}' \equiv \frac{d}{dT}\mathcal{Z}$, we obtain a similar equation to Eq. (26):

$$\delta T_n^* \simeq \frac{T_n^{*2}}{\mathcal{Z}'_n(T_n^*)\langle \Delta E \rangle_n (T_n^*)} \left[\frac{\mathcal{N}'^{(k)}_n}{N_{n_0}^{(k)}} g_{n_0} - \mathcal{Z}'_n(T_n^*)\right].$$

In the same limit $T_n \to 0$, both numerators and denominators are of $o(\epsilon)$ and the temperature iterations are again unstable; this was verified through extensive tests under a variety of conditions and configurations. To avoid this systematic numerical problem, we must consider another way to evaluate the Boltzmann temperature inside each group.

Consider instead the following expansion of the partition function near the mean relative energy value $\overline{\Delta E}_n = \frac{1}{g_n}\sum_{i \in n} g_i \Delta E_i$. Defining $\delta_i \equiv \Delta E_i - \overline{\Delta E}_n$ as the shifted energy gap, we have

$$\begin{aligned}\mathcal{Z}_n(T_n) &= \sum_{i \in n} g_i e^{-\Delta E_i/T_n} = e^{-\overline{\Delta E}_n/T_n} \sum_{i \in n} g_i e^{-\delta_i/T_n} \\ &= e^{-\overline{\Delta E}_n/T_n} \sum_{i \in n} g_i \left[1 - \frac{\delta_i}{T_n} + \frac{1}{2}\frac{\delta_i^2}{T_n^2} + \cdots\right] \\ &\simeq g_n e^{-\overline{\Delta E}_n/T_n}\left[1 + o(\langle \delta^2 \rangle / T_n^2)\right],\end{aligned} \tag{29}$$

where g_n is the total degeneracy—see Eq. (16). Therefore, up to second-order in the approximate ratio of the bin width to the temperature, the partition function can be approximated by a single exponential function and the relation (29) can be inverted. If we use the $(N_{n_0}, \mathcal{N})$ pair of conserved variables, we have

$$\frac{\mathcal{N}_n^{(k)}}{N_{n_0}^{(k)}} g_0 = \mathcal{Z}_n(T_n^{(k)}) \simeq g_n e^{-\overline{\Delta E}_n/T_n^{(k)}}. \tag{30}$$

However, the left-hand-side of Eq. (30) is $o(1+\epsilon)$, and the right-hand-side should be as well. To see that this is the case, consider the first terms in the expansion of Eq. (29)[28]

$$\mathcal{Z}_n(T_n) \simeq e^{-\overline{\Delta E}_n/T_n}\left[g_0 e^{-(\Delta E_0 - \overline{\Delta E}_n)/T_n} + g_1 e^{-(\Delta E_1 - \overline{\Delta E}_n)/T_n} + \cdots\right].$$

Since $\overline{\Delta E} \simeq \Delta E_1$ and $\Delta E_0 \equiv 0$, the right-hand-side is $o(\epsilon)[o(1/\epsilon) + 1 + \cdots] \simeq o(1+\epsilon)$. Again, this is not a

desirable situation, since the evaluation of the group temperature T_n is of the form $1/\ln(1+\epsilon)$, and is subject to significant errors. Furthermore, by computing the average gap $\overline{\Delta E}$ from the lower-bound of the energy bin, the requirement $\langle\delta\rangle \ll T_n$ may be hard to justify at low group temperature.

Instead, we can take advantage of the self-similar structure of the atomic spectrum (exact for hydrogen, approximate for other atoms) and the fact that the energy gaps become narrower as the level index increases. Thus, let us define the average energy counting from the first level *above* the lowest level, as obtained from $\mathcal{Z}'_n$, defined in Eq. (27)

$$\mathcal{Z}'_n = \sum_{i\in n'} g_i e^{-\Delta E_i/T_n} = e^{-\overline{\Delta E'}_n/T_n} \sum_{i>n_0} g_i e^{-\delta'_i/T_n}. \tag{31}$$

By definition of the mean, the first-order term in the expansion of the exponential on the right-hand-side should be: $\sum_{i\in n'} g_i\delta'_i = 0$, where now $\delta'_i \equiv \Delta E_i - \overline{\Delta E'_n}$. This yields

$$\overline{\Delta E'_n} = \frac{1}{g'_n}\sum_{i\in n'} g_i \Delta E_i \quad \text{with} \quad g'_n = \sum_{i>n_0} g_i. \tag{32}$$

Therefore, $\overline{\Delta E'}$ differs from $\overline{\Delta E}$ only by a normalization factor, since $\Delta E_0 \equiv 0$. Note that $\overline{\Delta E'} > \Delta E_1$ and to *lowest*-order, $\mathcal{Z}'(T_n) \simeq g'_n e^{-\overline{\Delta E'}/T_n} \simeq o(\epsilon)$. Using the conserved pair $(N_{n_0}, \mathcal{N}')$, the group temperature is now estimated by

$$\frac{\mathcal{N}'^{(k)}_n}{N^{(k)}_{n_0}} g_{n_0} = \mathcal{Z}'_n(T_n) \quad \rightarrow \quad T^{(k)}_n \simeq -\frac{\overline{\Delta E'_n}}{\ln\left[\dfrac{\mathcal{N}'_n}{g'_n}\dfrac{g_{n_0}}{N_{n_0}}\right]} \simeq -\frac{1}{\ln(\epsilon)}. \tag{33}$$

This is now a stable computation when $\epsilon \rightarrow 0$. Furthermore, the approximation $\langle\delta\rangle \ll T_n$ is more justifiable since the largest value ($\delta_0 = E_{n_0} - \overline{\Delta E}$) is removed from the average.

We see that we now have the means to compute the internal group temperature from conserved variables without risking fatal numerical errors; this is possible *only* by separating the lowest and upper levels within the group, i.e., by performing a sub-scale, internal partitioning of the group.[29] This is the approach used here for the last Boltzmann (hereafter denoted as B5) group we investigated, for which the appropriate pair of conserved variables to use is therefore $(N_{n_0}, \mathcal{N}'_n)$. Note that it is also possible to improve on the temperature evaluation by incorporating all higher-order terms into the definition of the total degeneracy, i.e.,

$$\mathcal{Z}'_n(T_n) = \tilde{g}'_n(T_n) e^{-\overline{\Delta E'_n}/T_n}$$
$$\rightarrow \frac{d\mathcal{Z}'_n}{dT_n} = \mathcal{Z}'_n(T_n)\cdot\left[\frac{\overline{\Delta E'_n}}{T_n^2} + \frac{d}{dT_n}\ln\tilde{g}'_n\right]. \tag{34}$$

If T^*_n is the running iteration, first evaluated by Eq. (33), successive estimates of $T^{(k)}_n$ are obtained, using Eq. (34), from:

$$T^{(k)}_n - T^*_n = \frac{\ln\mathcal{Z}'_n(T^{(k)}_n) - \ln\mathcal{Z}'_n(T^*_n)}{\left[\dfrac{d\ln\mathcal{Z}'_n}{dT_n}\right](T^*_n)} \quad \text{where}$$
$$\mathcal{Z}'_n(T^{(k)}_n) = g_{n_0}\frac{\mathcal{N}'^{(k)}_n}{N^{(k)}_{n_0}}. \tag{35}$$

This iterative procedure can rapidly converge (as demonstrated in our tests) because we have an excellent approximation of the initial temperature from the lowest-order direct evaluation (33), and the $o(\epsilon)$ term has been factored as the leading term in the expansion. In other words, $\tilde{g}'_n(T_n)$ is a smooth function of temperature with a non-vanishing gradient, allowing gradient-descent iterations.

D. Boltzmann grouping—Effective rates

As before, the master equations are used to derive the conservation equations for the two new variables $(N_{n_0}, \mathcal{N}'_n)$, by setting $i = n_0$ for the first one, and summing over all levels $j \in n'$ in the second case. The latter yields the following:

$$\begin{aligned}
\frac{d\mathcal{N}'_n}{dt} = &-N_e\mathcal{N}'_n\left[\sum_{m>n}\sum_{i\in n'}\frac{g_i e^{-\Delta E_i/T_n}}{\mathcal{Z}'_n}\sum_{j\in m}\alpha_{(j|i)} + \sum_{m<n}\sum_{i\in n'}\frac{g_i e^{-\Delta E_i/T_n}}{\mathcal{Z}'_n}\sum_{j\in m}\beta_{(j|i)}\right]\\
&+N_e\mathcal{N}_m\left[\sum_{m<n}\sum_{i\in n'}\sum_{j\in m}\frac{g_j e^{-\Delta E_j/T_m}}{\mathcal{Z}_m}\alpha_{(i|j)} + \sum_{m>n}\sum_{i\in n'}\sum_{j\in m}\frac{g_j e^{-\Delta E_j/T_m}}{\mathcal{Z}_m}\beta_{(i|j)}\right]\\
&-\mathcal{N}'_n\left[\sum_{m<n}\sum_{i\in n'}\frac{g_i e^{-\Delta E_i/T_n}}{\mathcal{Z}'_n}\sum_{j\in m}A_{(j|i)}\right] + \mathcal{N}_m\left[\sum_{m>n}\sum_{i\in n'}\sum_{j\in m}\frac{g_j e^{-\Delta E_j/T_m}}{\mathcal{Z}_m}A_{(i|j)}\right]\\
&-N_e\mathcal{N}'_n\left[\sum_{i\in n'}\frac{g_i e^{-\Delta E_i/T_n}}{\mathcal{Z}'_n}\beta_{(n_0|i)} + \sum_{i\in n'}\frac{g_i e^{-\Delta E_i/T_n}}{\mathcal{Z}'_n}A_{(n_0|i)}\right] - N_e\mathcal{N}'_n\left[\sum_{i\in n'}\frac{g_i e^{-\Delta E_i/T_n}}{\mathcal{Z}'_n}\alpha_{(+|i)}\right] + N_e^2 N_+\left[\sum_{i\in n'}\beta_{(i|+)}\right].
\end{aligned} \tag{36}$$

Note that we have used the total number $\mathcal{N}_m = N_{m_0} + \mathcal{N}'_m$ and the group total partition function $\mathcal{Z}_m = g_{m_0} + \mathcal{Z}'_m$ in the expressions on the right hand side, only as a way to group terms and lead to simpler expressions; the conserved variables remain N_{m_0} and $\mathcal{N}'_m$. Equation (36) takes in account all the interactions between the groups, assuming the Boltzmann distribution approximation within each group. The effective rates for group transitions can be expressed

(and tabulated) as a function of two temperatures: the kinetic temperature T_e and the group excitation temperature T_n. Notice also that because of the bin-averaging, the effective radiative transition rates have also become temperature-dependent (T_n).

Similarly, the rate of change of the number density of the ground state of each group is

$$\begin{aligned}\frac{dN_{n_0}}{dt} = &-N_e N_{n_0}\left[\sum_{m>n}\sum_{j\in m}\alpha_{(j|n_0)} + \sum_{m<n}\sum_{j\in m}\beta_{(j|n_0)}\right]\\ &+N_e\mathcal{N}_m\left[\sum_{m<n}\sum_{j\in m}\frac{g_j e^{-\Delta E_j/T_m}}{\mathcal{Z}_m}\alpha_{(n_0|j)}\right.\\ &\left.+\sum_{m>n}\sum_{j\in m}\frac{g_j e^{-\Delta E_j/T_m}}{\mathcal{Z}_m}\beta_{(n_0|j)}\right] - N_{n_0}\left[\sum_{m<n}\sum_{j\in m}A_{(j|n_0)}\right]\\ &+\mathcal{N}_m\left[\sum_{m>n}\sum_{j\in m}\frac{g_j e^{-\Delta E_j/T_m}}{\mathcal{Z}_m}A_{(n_0|j)}\right]\\ &+N_e\mathcal{N}'_n\left[\sum_{i\in n'}\frac{g_i e^{-\Delta E_i/T_n}}{\mathcal{Z}'_n}\beta_{(n_0|i)} + \sum_{i\in n'}\frac{g_i e^{-\Delta E_i/T_n}}{\mathcal{Z}'_n}A_{(n_0|i)}\right]\\ &-N_e N_{n_0}\left[\alpha_{(+|n_0)}\right] + N_e^2 N_+\left[\beta_{(n_0|+)}\right]. \end{aligned} \tag{37}$$

Again, using the total number of levels $\mathcal{N}_m = N_{m_0} + \mathcal{N}'_m$ on the right-hand-side allows us to consider together transitions between lowest states at the boundaries of different groups ($N_{n_0} - N_{m_0}$), as well as the transitions with the excited sub-partitions ($N_{n_0} - \mathcal{N}'_m$) and simply the expressions. Since the ion is conserved here as an individual state, the rate of change of its number density remains the same but can be rewritten in terms of the group number densities

$$\begin{aligned}\frac{dN_+}{dt} = &N_e\sum_n \mathcal{N}_n\left[\sum_{i\in n}\frac{g_i e^{-\Delta E_i/T_n}}{\mathcal{Z}_n}\alpha_{(+|i)}\right]\\ &-N_e^2 N_+\left[\sum_n\sum_{i\in n}\beta_{(i|+)}\right]. \end{aligned} \tag{38}$$

Each term in brackets in Eqs. (36)–(38) is an effective rate for transfer between the group variables $(N_{n_0}, \mathcal{N}'_n), \forall n$. As mentioned in Sec. III A, both individual levels and groups (uniform or Boltzmann) are considered when solving the ASDF. The few individual states are the lowest in the energy scale, with the largest successive gaps, while the multitude of upper levels is distributed into a variable number of groups. This is justified on the basis of the kinetic rates (see the stiffness ratios of Figure 1), and as justification of the expansion (29).

IV. ACCURACY OF UNIFORM AND BOLTZMANN METHODS

A. Isothermal ionization test case

In the previous section, we have discussed several approaches to the level grouping strategy; these are summarized in Table I. This sequence of models was developed as a result of preliminary tests and the failure to obtain converged solutions for the group Boltzmann temperature T_n in many instances. Thus, we found that the *only* model which was able to provide stable and satisfactory solutions for all test cases was model B5, using a sub-partition of the group into the ground level n_0 and the remainder, and the use of the form (31) for the partition function, which allowed us to factorize out the vanishingly small terms at low T_n. Therefore, considerations of the "equation of state" of the Boltzmann group dictated the correct approach to use here, and while all the models explored are listed in Table I, only the zeroth-order uniform binning described in Sec. III A and the B5 models are shown here and compared to the reference solution obtained from solving the full master equations; these are indicated as (U) and (B) models, respectively.

TABLE I. Summary of level-grouping models investigated.

Model	Variables	Equations	T_n evaluation
U	$\mathcal{N}_n$	(18) and (19)	none
B1	$(\mathcal{N}_n, \mathcal{E}_n)$	(20a), (20b), and (38)	C_v—unstable
B2	$(N_{n_0}, \mathcal{N}_n)$	(37) and (20a)	C_v—unstable
B3	$(N_{n_0}, \mathcal{N}'_n)$	(37) and (36)	C_v—unstable
B4	$(N_{n_0}, \mathcal{N}_n)$	(37) and (20a)	Eq. (29)—unstable
B5	$(N_{n_0}, \mathcal{N}'_n)$	(37) and (36)	Eq. (31)—stable

We conducted a large number of additional tests but for the sake of brevity, we are showing here the results of three representative cases: the initial conditions are summarized in Table II. For all the results shown in this section, a constant time step of 10^{-7} s had been used for the test cases in the ionization regime (cases 1 and 3), and a time step of 10^{-5} s was used for the recombination regime (case 2); the same backward-Euler scheme of Sec. II C was used throughout.

As indicated in Sec. III, the reference solution is based on the detailed kinetics for 20 atomic levels, while the group-based solutions will be based on a few low energy levels individually monitored, and with partitioning of the remaining upper states into a variable number of groups. The first test case is the iso-thermal relaxation in the excitation and ionization regime, i.e., the initial population of excited states and electron density is well below equilibrium.[30] This test case is the same as the one shown in Figure 2 for a variable number of electronic levels, solving for the full master equations (8) and (9). As the plasma relaxes towards equilibrium, an increasing number of electronic levels become populated and the electron number density grows exponentially, until an ionization cascade occurs. The rates increase very rapidly just before equilibrium, and the system becomes very stiff, as shown by the large spread of eigenvalues in Figure 1.

TABLE II. Initial conditions of test cases. For all cases, the total atomic density N_H is 10^{21} m^{-3}.

Case	T_e	$x_e = N_+/N_H$	N_n	
1	3 eV—isothermal	10^{-9}	$(1-x_e)N_H$	for n = 1
			$10^{-20}N_H$	otherwise
2	1 eV—isothermal	Saha (3 eV)	Boltzmann (3 eV)	
3	3 eV—isochoric	10^{-9}	$(1-x_e)N_H$	for n = 1
			$10^{-20}N_H$	otherwise

Figure 3 shows a comparison of the number densities of all the atomic states for the iso-thermal test case (1). In this simulation, the ground state and the first 4 excited states (1,…,5) are conserved as discrete levels while the remaining upper states (6,…,20) are partitioned into two groups, each of which has either a uniform or Boltzmann distribution. There are both significant and subtle differences in the traces

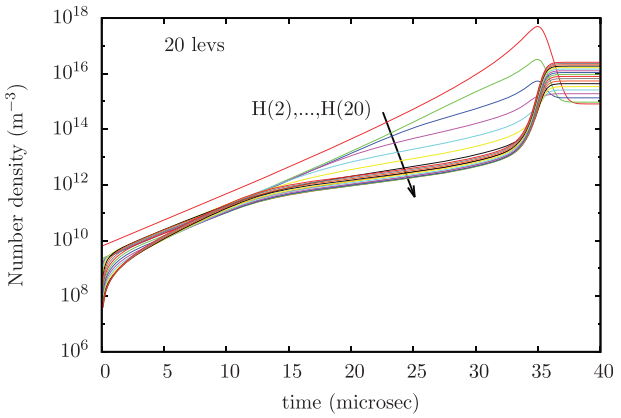

(a) Full solution with 20 levels.

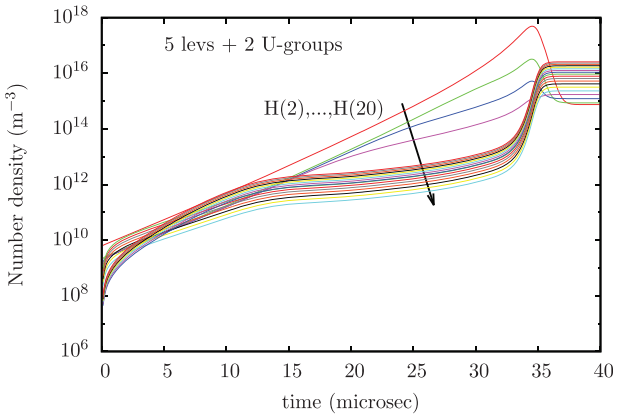

(b) Solution with 5 levels and 2 Uniform groups

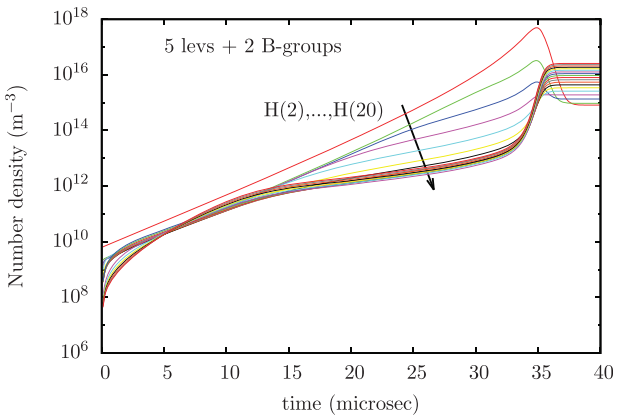

(c) Solution with 5 levels and 2 Boltzmann groups.

FIG. 3. Comparison of the time evolution of the excited states during the isothermal heating test case ($T_e = 3$ eV). From top to bottom: (a) full solution with 20 levels; (b) solution with 5 levels and 2 uniform groups; (c) solution with 5 levels and 2 Boltzmann groups. The first excited state—H(2)—is the top curve, followed by the next higher level, etc.

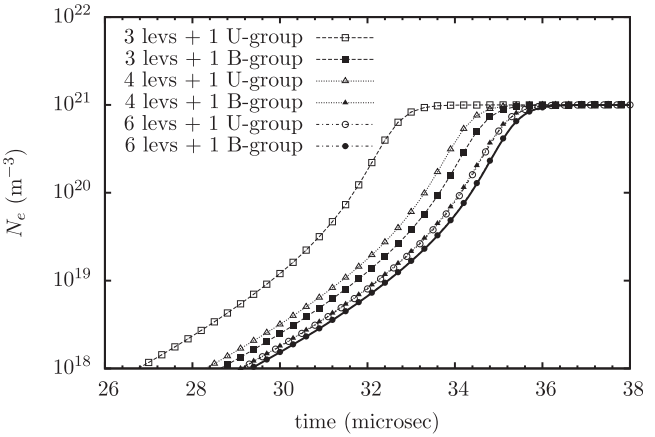

FIG. 4. Comparison between the solution obtained using both level grouping approaches. The solid line represents the full solution.

of the upper states. First, comparison of the uniform (Figure 3(b)) and Boltzmann (Figure 3(c)) grouping shows the influence of the assumed internal distribution, as the reconstructed levels of the groups are clearly separated in the uniform case. Second, comparison with the reference solution of Figure 3(a) shows that the Boltzmann groups are clearly more accurate. Slight differences remain in the very early stages of evolution[31] below 1 μs for example and around 10 μs.

The combined effect of the number of resolved lower levels and grouping strategy is shown in Figure 4. Generally speaking, one can clearly observe a dramatic improvement, for the same number of resolved levels, by switching from a uniform to Boltzmann group.[32] By selecting the time of maximum rate of growth of the electron density as the approximate location of the avalanche ionization, we can measure the relative error in density. As shown in Table III, the error can be very substantial unless there is sufficient resolution of the ASDF kinetics, through the number of resolved lower levels and a higher-order (B) description of the groups. This is important when comparing, for example, with time-gated experimental results.

By conserving more discrete states and reducing the size of the upper state groups, the results are of course significantly improved. This is to be expected for ASDF kinetics, since the energy gaps are larger for the first levels, and grouping together these states would be less accurate, first by yielding excessive bin energy widths compared to mean energy and temperature scale—violating the validity condition for the expansion (29)—and also by disallowing

TABLE III. Relative error on electron density at peak rate of growth (approximately 33 μs).

Method	Error (%)
3 levels + 1 U-group	2618
3 levels + 1 B-group	89.2
4 levels + 1 U-group	165.8
4 levels + 1 B-group	23.7
6 levels + 1 U-group	20.9
6 levels + 1 B-group	0.9

potential deviations from Boltzmann equilibrium in the most populated range of excited states.

There can of course be variations in the grouping strategy, but in all cases the general guidelines of keeping the *widths* of the groups small and the levels with the largest energy gaps as individual states are perfectly consistent with the objective of computational cost reduction, since the discrete lower energy states evolve more slowly and the upper states are numerous and have similar energy.[33]

The relative accuracy of the grouping approaches can also be seen in Figure 5 where the ASDF is plotted at four different instances of time corresponding to $t = 10$, 20, 30, and 40 μs. Both solutions with level grouping are obtained from using 3 atomic levels and 1 group of upper states. It is clearly seen that the Boltzmann group gives a more accurate representation of the upper states distribution during the heating process. We also showed in Figure 5 the results of a simplified model where it is assumed (see Sec. III B) that all groups have the same internal temperature, equal to the kinetic temperature, i.e., $T_b(n) \equiv T_e, \forall n$ (dashed line). This assumption is clearly violated, as shown in Figure 6, although the difference remains mostly confined to the upper states distribution. We should point out again that significant differences would be expected in a two-temperature kinetic system, i.e., including heavy-particle collisions.

We note also that the ASDF from the full solution indicates that the high lying states, starting from the third excited state, behave like a continuum state, although there appears to be two distinct sub-groups among the upper states, as can be seen most clearly at $t = 10$ μs. This suggests that the upper states are most effectively resolved by two groups or more, again confirming that relatively small widths of the groups are preferable, albeit at an increased computational expense. Figure 6 further illustrates this point by showing the evolution of the Boltzmann temperatures of the upper states, using here 4 discrete atomic states and partitioning the upper states into 3 groups. While the Boltzmann temperatures of the first two groups are close to each other, the temperature of the third group is slightly higher. This again confirms that the upper states need to be resolved by at least 2 groups. When the system is near equilibrium, both approaches give similar results.

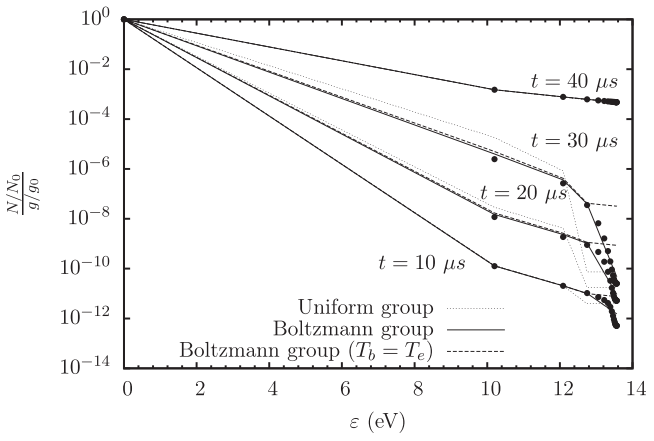

FIG. 5. The internal states population during the heating process at various times. The solid symbols are the full solution; the solid lines are the level grouping with Boltzmann distribution; the doted lines are for level grouping with uniform distribution; dashed lines are for a simplified model with $T_b \equiv T_e$.

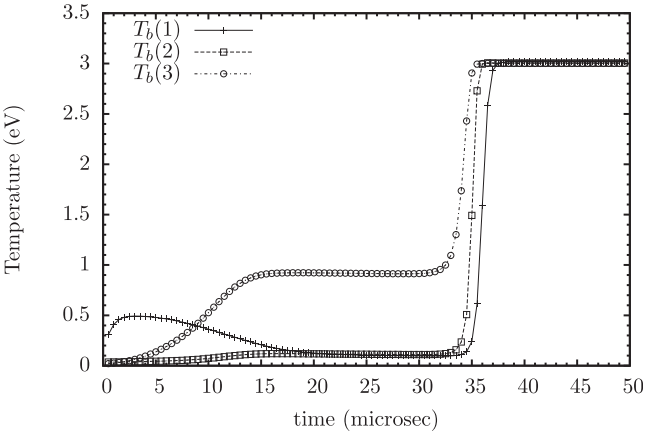

FIG. 6. Boltzmann temperature of the upper states.

In these simulations, we have assumed that the plasma is optically thin to all the radiation from the line transitions. Spectral signatures being a major diagnostic tool for determining plasma conditions, it is important to know the CR kinetics in detail in order to match experimental data. Usually, this is accomplished by post-processing the numerical solution with a highly resolved spectral code—including radiation transport (RT) if necessary—with detailed computation of line shapes. This approach is accurate if the key parameters of such a spectral model, in particular N_e and T_e, are also very accurate. As discussed above and shown in Table III, our Boltzmann grouping procedure provides a significant improvement over conventional approaches, leading to a potentially much more accurate spectral signature prediction in transient and non-equilibrium plasma conditions. In addition, the ASDF solution is much closer to the true physical state, which may also lead to faster integration of the detailed CR kinetics with RT. These will be investigated in the future.

Accurate evaluation of the radiative emission is also important during the computation of flow dynamics, from simple reasons of power coupling, e.g., radiative cooling. Figure 7 shows the radiative losses due to bound-bound radiation from the upper states (5,…,20) to the first three atomic states (1, 2, 3) computed by grouping all the upper states together as a single group with a Boltzmann distribution. Although this is a somewhat coarse approximation to the ASDF, it is clear that the grouping scheme provides an excellent approximation to the radiative power. An accurate reproduction of the radiative spectrum depends inevitably on the reconstructed population of the atomic levels and, as can be seen by comparing the profiles in Figure 3, the agreement can be excellent.

B. Isothermal recombination test case

In this case, we performed a cooling test where the plasma is suddenly brought down from 3 eV to 1 eV. Thus, the simulation was run at a constant temperature ($T_e = 1$ eV), while the initial conditions are the Boltzmann and Saha equilibrium values at 3 eV; these are exactly the conditions which would be obtained at the end of the first test case in

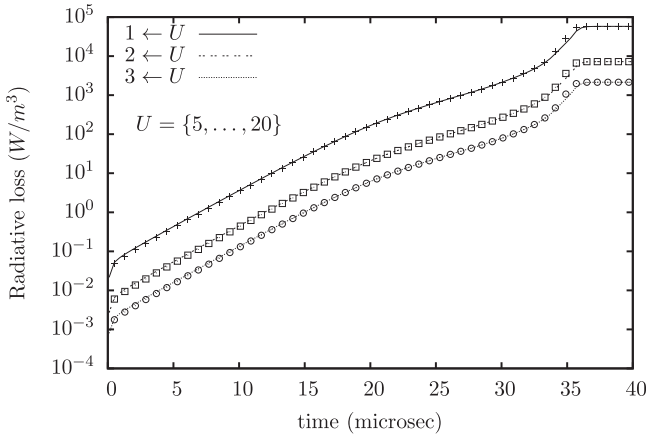

FIG. 7. Radiative loss due to bound-bound radiation from the upper states to the first 3 atomic states. The lines indicate the solution obtained from the full CR kinetics. The dots represent solution obtained with level grouping (5 levels + 1 group).

the absence of radiative losses. For all the simulations shown in this case, a constant time step of 10^{-5} s has been used.

In this case, the cooling process occurs very rapidly and the plasma is in a deexcitation and recombination regime; the ground state and the electron number densities are quickly adjusted to their new equilibrium values, as can be seen in Figure 8. Strictly speaking, since bound-bound radiation is assumed to be optically thin, the system cannot reach equilibrium. However, a quasi-equilibrium state is achieved at approximately 1 ms, after which the bound-bound radiation is the dominant *net* rate of change and the system continues to cool down at the radiative time scales. Note also that the uniform grouping is significantly less time-accurate than the Boltzmann method, as was already the case in the ionization regime—see Figure 4.

Figure 9 shows the evolution of the excited states as function of time for reference, uniform groups and Boltzmann groups. Once again, there is a noticeable discrepancy between the reference solution and the uniform bin model, especially concerning the red curve which crosses other levels during the relaxation process. This curve is the density of H(2), the first excited state, and is an effect of the

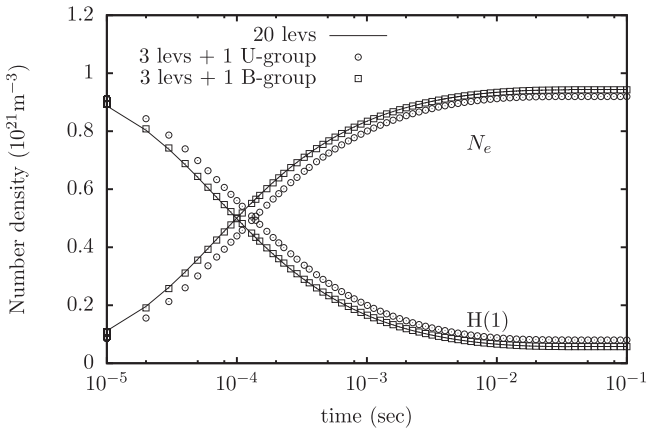

FIG. 8. Comparison of the time evolution of the ground state and the free electrons during the isothermal cooling process (3 eV → 1 eV) using level grouping with uniform and Boltzmann distribution (3 levels + 1 group).

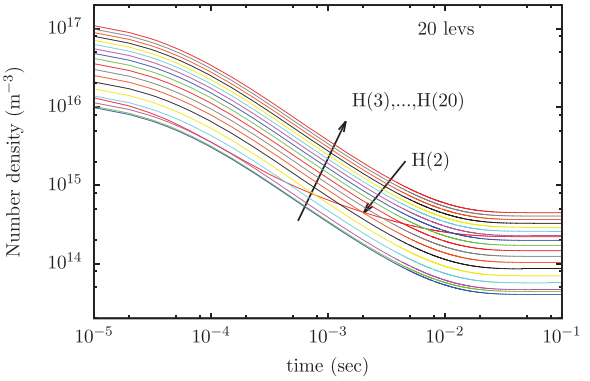

(a) Full solution with 20 levels.

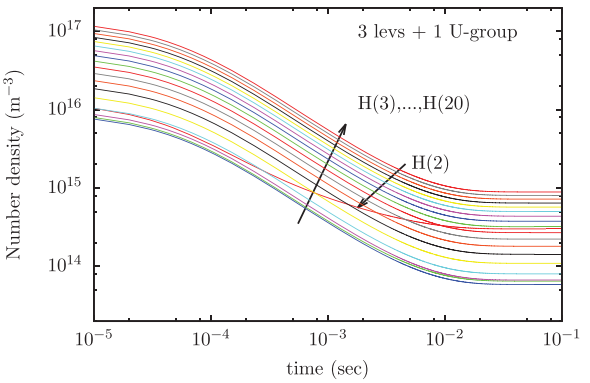

(b) Solution with 3 levels and 1 Uniform group

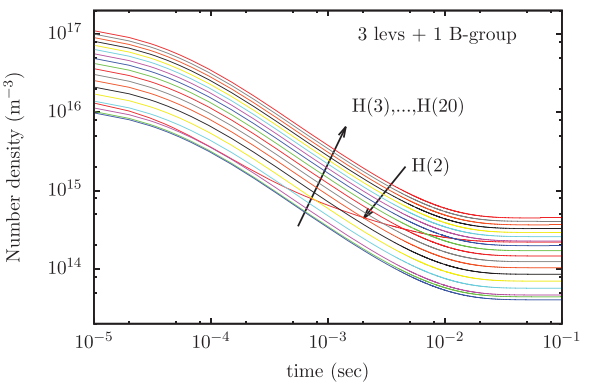

(c) Solution with 3 levels and 1 Boltzmann group.

FIG. 9. Comparison of the time evolution of the excited states during the isothermal cooling test case ($T_e = 1$ eV). From top to bottom: (a) full solution with 20 levels; (b) solution with 3 levels and 1 uniform group; (c) solution with 3 levels and 1 Boltzmann group. H(3)—is the bottom curve, followed by the next higher level, etc.; the non-conforming red curve is H(2). The higher population densities as the level index increases include the increase of the level degeneracy.

strong radiative decay of this state. Notice that the plot starts at $t = 10^{-5}$ s, i.e., the first implicit time step, but already the solution is far from the Boltzmann equilibrium which is the initial condition at $t = 0$, such that there is a population inversion with respect to H(2) for many upper states. Notice also that the time scale is logarithmic, and the processes considerably slow down as the electron density drops significantly. Because we are considering only electron impact collisions, the ASDF essentially becomes "frozen" in a quasi-static but

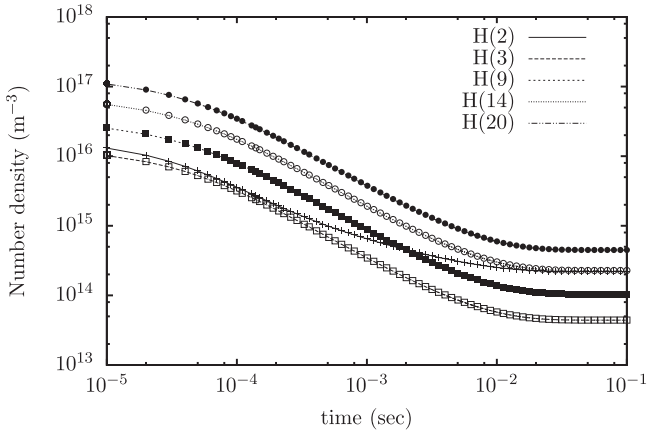

FIG. 10. Comparison of the time evolution of the excited states number densities during the isothermal cooling process. The lines are full solution. The dots represent solution obtained with level grouping (3 levels + 1 B group).

non-equilibrium state. If collisions by heavy particles were also considered, these would rapidly become the dominant process, leading to faster relaxation towards equilibrium. However, in some case of rapid plasma expansion, similar "frozen-in" non-equilibrium distribution functions of the ASDF could be obtained.

To better appreciate the accuracy of the Boltzmann grouping procedure, Figure 10 shows the evolution of several excited states compared to the exact solution and similarly to the "heating" (ionization) case, excellent agreement was obtained. In this simulation, the first 3 atomic states (1, 2, 3) are conserved as discrete levels and the upper states (4,…,20) are lumped into 1 Boltzmann group.

Finally, we show in Figure 11 the snapshots of the ASDF during the recombination. Contrary to the case of ionization, the upper states are not depleted but enhanced instead—as expected, since the recombination proceeds preferentially onto the upper states. As a reflection of the observation made for Figure 10, the agreement is excellent for all atomic states.

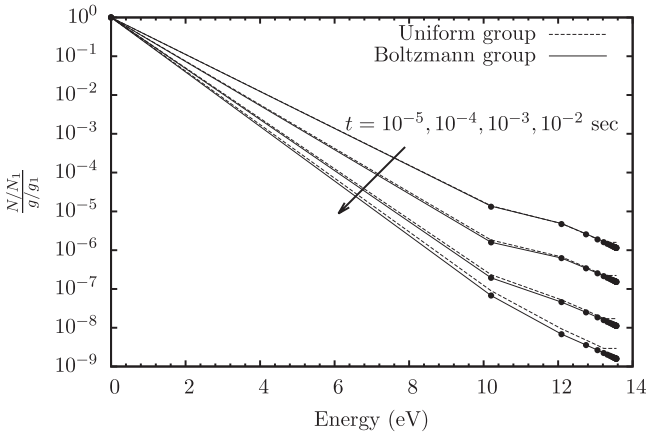

FIG. 11. Snapshots of the ASDF at several times during the cooling process. The dots represent the full solution. The solid lines are the solution obtained using the level grouping with Boltzmann distribution. The broken lines are the solution obtained using the level grouping with uniform distribution.

V. ENERGY CONSERVATION

A. Effective rates

The systems of equations (18)–(19) and (36)–(38) describe the complete evolution of the ASDF but for an isothermal plasma. In the more general case, the ASDF kinetics are coupled to the energy of the system; here, this includes only the total energy of the free electrons E_e. Thus for constant-volume or constant-pressure conditions, there must be an evolution equation for the energy or enthalpy (only constant-volume kinetics are considered here). We must then exert care that the formulation exactly conserves energy, i.e., that $E_e^{(k)} + \sum_n \mathcal{E}_n^{(k)}$ at any time level (k) remains the same within numerical round-off errors. If we were dealing with only electron-impact collisions, it would be sufficient to sum the energies of all levels using the new population densities at the end of the time step, compute the difference and assign the change to E_e. However, there are two obvious problems with this scenario: (a) when other collision partners must be accounted for, or when the electrons themselves are partitioned (e.g., for non-Maxwellian kinetics), one must be able to correctly apportion the changes in energy, e.g., to E_e and E_h (for heavy particles) and (b) for large time steps, there is no guarantee that the subsequent change in E_e is physically acceptable, i.e., $E_e^{(k)} = E_e^{(k-1)} + \delta E_e > 0$. We must therefore include an evolution equation for E_e (and another for E_h if heavy particle collisions are included), which must then be fully coupled, so that the Jacobian of the system (14) includes derivatives of the rates with respect to E_e, through the variation of T_e.

Energy conservation can be satisfied if the construction of the source term on the right-hand-side of the master equations also satisfies it. Thus, we must explicitly construct the energy source term from the master equations, as was already described briefly in Eq. (20). The same procedure is used, with the understanding that

$$\frac{dE_e}{dt} = -\sum_n \frac{d\mathcal{E}_n}{dt}.$$

Thus we can combine contributions as follows:

$$\frac{dE_e}{dt} = -N_e \mathcal{N}_n \left[\sum_{\substack{m>n \\ i\in n}} \frac{g_i e^{-\Delta E_i/T_n}}{\mathcal{Z}_n} \sum_{j\in m} \Delta E_{ji} \alpha_{(j|i)} + \sum_{\substack{m<n \\ i\in n}} \frac{g_i e^{-\Delta E_i/T_n}}{\mathcal{Z}_n} \sum_{j\in m} \Delta E_{ji} \beta_{(j|i)} \right] \ldots, \tag{39}$$

where $\Delta E_{ji} = E_j - E_i$. Note that in the case of excitation from level $|i)$, i.e., the first summation in Eq. (39), $\Delta E_{ji} > 0$, while $\Delta E_{ji} < 0$ in the second term for de-excitations from that level. We can then construct another set of effective rates, this time for the energy equation. Using the subpartitioning of model B5, the rates derived from the first term on the right of Eq. (36) are

$$\tilde{\alpha}^E_{(m'|n')} = \left[\sum_{i\in n'} \frac{g_i e^{-\Delta E_i/T_n}}{\mathcal{Z}'_n} \sum_{j\in m'} \Delta E_{ji}\alpha_{(j|i)}\right], \tag{40a}$$

$$\tilde{\beta}^E_{(m'|n')} = \left[\sum_{i\in n'} \frac{g_i e^{-\Delta E_i/T_n}}{\mathcal{Z}'_n} \sum_{j\in m'} \Delta E_{ji}\beta_{(j|i)}\right]. \tag{40b}$$

These rates enter the evolution equation for E_e as

$$\frac{dE_e}{dt} = -N_e\mathcal{N}'_n \sum_{m>n} \tilde{\alpha}^E_{(m'|n')} - N_e\mathcal{N}'_n \sum_{m<n} \tilde{\beta}^E_{(m'|n')} + \cdots. \tag{41}$$

Note that the same formulation applies for uniform groups by taking the limit $T_n \to \infty$, and summing over the complete set $n = \{n_0, n'\}$. The rate of energy change can also be expressed as

$$\tilde{\alpha}^E_{(m'|n')} = \tilde{\alpha}_{(m'|n')} \cdot \bar{\varepsilon}_{(m'|n')}, \tag{42}$$

where $\alpha_{(m'|n')}$ is of course given by the effective rate for the conserved number densities

$$\tilde{\alpha}_{(m'|n')} = \sum_{j\in m'} \sum_{i\in n'} \frac{g_i e^{-\Delta E_i/T_n}}{\mathcal{Z}'_n} \alpha_{(j|i)}.$$

Equation (42) defines an average energy $\bar{\varepsilon}_{(m'|n')}$, transferred during excitation of levels of group n' to levels of group m', which can be tabulated as function of the initial T_n and collisional (T_e) temperatures. This approach was successfully used, for example, for vibrational non-equilibrium.[34]

B. Isochoric ionization test case

The third test case of Table II was designed to test for energy conservation. In this case, the energy loss and gain due to collisional processes are taken into account in the conservation equation for the electron energy. The evolution now proceeds at constant volume, and the electron temperature changes rapidly, as seen in Figure 12. The initial conditions are the same as those of the first test case, and the system is initially far below Boltzmann and Saha equilibrium However, contrary to the isothermal case, the initial excitation and ionization processes deplete the electron energy and the system "freezes" rapidly, and the excited states remain at a low population density. If an external heating source was applied (e.g., Ohmic heating), the system would more closely resemble the isothermal test case, and the system would become stiff again. Here, we are mostly concerned with testing energy conservation and to simplify the analysis, the radiative rates were removed from the kinetics, so that no radiative energy losses were present.

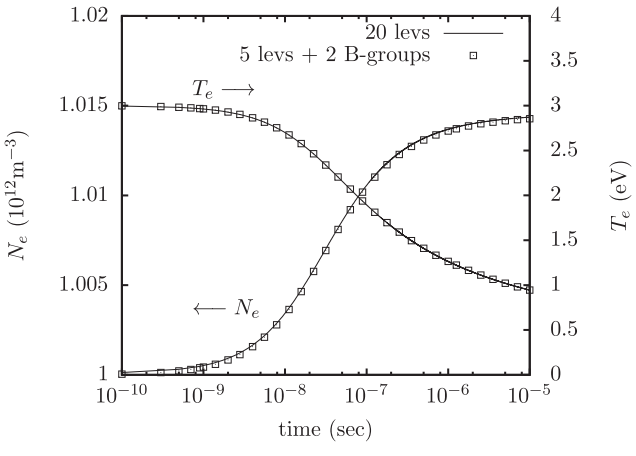

FIG. 12. N_e, T_e evolution in constant-volume case.

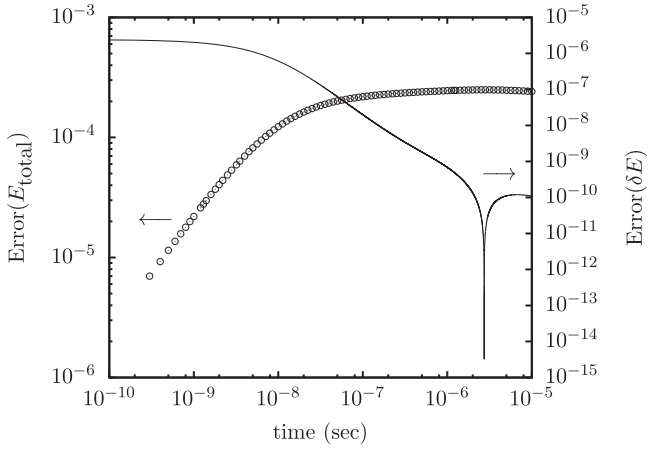

FIG. 13. Cumulative and instantaneous relative errors in energy conservation—test case 3.

We can monitor the error by comparing the values of E_e at the end of each time step with the total potential energy contained in the electronic states, by reconstruction of the level populations. Figure 13 shows both the accumulated error (symbols) and the one at each time step (solid line); this test was conducted with 5 resolved levels and 2 Boltzmann groups, and all computations were performed with a constant time step of 10^{-10} s, using the same backward-Euler integration scheme.[35]

The error is certainly acceptable, but it is not commensurate with numerical round-off, which we would have expected if the scheme was exactly energy-conserving. By comparison, the cumulative error in energy was below 10^{-13} when solving the full master equations without level grouping.

While the exact solution consists of summing-up the contributions from each individual level, leading to the rate of change expressed by Eq. (20b). However, we are not using here the internal energy $\mathcal{E}_n$ as a conserved variable, and we must be careful that the procedure be consistent with our definition, or *reconstruction* of the internal energy. The corrected procedure is described next.

C. Corrected energy rates

Consider for example the change in electron energy due to excitations and de-excitations, and let us examine first the case of uniform grouping.

$$\frac{dE_e}{dt} = -\sum_{m>n}\sum_{n} \tilde{\alpha}^E_{(m|n)}\mathcal{N}_n N_e + \sum_{m>n}\sum_{n} \tilde{\beta}^E_{(n|m)}\mathcal{N}_m N_e. \tag{43}$$

There are two formulations of the effective rates of energy transfer:

Formulation 1:

$$\tilde{\alpha}^E_{(m|n)} = \sum_{j\in m}\sum_{i\in n}\frac{g_i}{g_n}(E_j - E_i)\alpha_{(j|i)}, \tag{44a}$$

$$\tilde{\beta}^E_{(m|n)} = \sum_{j\in m}\sum_{i\in n}\frac{g_j}{g_m}(E_j - E_i)\beta_{(i|j)}. \tag{44b}$$

Formulation 2:

$$\tilde{\alpha}^E_{(m|n)} = (\tilde{E}_m - \tilde{E}_n)\sum_{j\in m}\sum_{i\in n}\frac{g_i}{g_n}\alpha_{(j|i)}, \tag{45a}$$

$$\tilde{\beta}^E_{(m|n)} = (\tilde{E}_m - \tilde{E}_n)\sum_{j\in m}\sum_{i\in n}\frac{g_j}{g_m}\beta_{(i|j)}, \tag{45b}$$

where $\tilde{E}_n = \sum_{i\in n}\frac{g_i}{g_n}E_i$ and similarly for $\tilde{E}_m$.

Only the second formulation is exactly energy-conserving. This is quite clear because in that case, the term on the right side of Eq. (45) is the product of the change in number density of the groups ($d\mathcal{N}_n/dt$) and the difference in average group energy ($\tilde{E}$). Energy conservation follows from the definition of the total group energy $\mathcal{E}_n = \tilde{E}_n\mathcal{N}_n$. Thus, the model assumptions *constrain* us to choose the appropriate formulation of the effective rates for energy change that is consistent with the definition of group energy.

Let us now examine the case of the Boltzmann grouping (B5), using the pair of conserved variables $(N_{n_0}, \mathcal{N}'_n)$; the rates of energy exchange must therefore be consistent with the electronic energy defined from these two variables, and with the equation of state used to describe the internal partition (i.e., T_n). We start with the conservation of the group energy

$$\begin{aligned}\frac{d\mathcal{E}_n}{dt} &= \frac{d}{dt}\left(N_{n_0}E_{n_0} + \mathcal{N}'_n\langle E\rangle_{n'}\right)\\ &= E_{n_0}\frac{dN_{n_0}}{dt} + \langle E\rangle_{n'}\frac{d\mathcal{N}'_n}{dt} + \mathcal{N}'_n\frac{d\langle E\rangle_{n'}}{dt}.\end{aligned} \tag{46}$$

Note that the averaging $\langle\rangle_{n'}$ is done for the remaining levels above the ground level n_0 of that group. We can write a similar equation for the total energy measured from the ground state of that group, i.e.,

$$\begin{aligned}\frac{d\Delta\mathcal{E}_n}{dt} \equiv \sum_{i\in n}\Delta E_i\frac{dN_i}{dt} &= \frac{d}{dt}\left(\mathcal{N}'_n\langle\Delta E\rangle_{n'}\right)\\ &= \langle\Delta E\rangle_{n'}\frac{d\mathcal{N}'_n}{dt} + \mathcal{N}'_n\frac{d\langle\Delta E\rangle_{n'}}{dt}.\end{aligned} \tag{47}$$

The first term in Eq. (47) describes the change in group energy from the global change in population of the group, i.e., $\langle E\rangle_n d\mathcal{N}_n/dt$. The last term describes the change of the internal structure of the group as a result of the collisional transitions, since

$$\frac{d\langle\Delta E\rangle_{n'}}{dt} = \frac{1}{T_n^2}\left[\langle\Delta E^2\rangle_{n'} - \langle\Delta E\rangle^2_{n'}\right]\frac{dT_n}{dt} = C_{v,n'}\frac{dT_n}{dt}. \tag{48}$$

From Eq. (31),

$$\frac{d\mathcal{Z}'_n}{dt} = \frac{g_{n_0}}{N_{n_0}}\left[\frac{d\mathcal{N}'_n}{dt} - \frac{\mathcal{N}'_n}{N_{n_0}}\frac{dN_{n_0}}{dt}\right] = \mathcal{Z}'_n\left[\frac{\overline{\Delta E}_n}{T_n^2} + \frac{d\ln\tilde{g}'_n}{dT_n}\right]\frac{dT_n}{dt}. \tag{49}$$

Inserting into Eq. (47),

$$\mathcal{N}'_n\frac{d\langle\Delta E\rangle_{n'}}{dt} = \frac{C_{v,n'}T_n^2}{\left(\overline{\Delta E'}_n + T_n^2\dfrac{d\ln\tilde{g}'_n}{dT_n}\right)}\left[\frac{d\mathcal{N}'_n}{dt} - \frac{\mathcal{N}'_n}{N_{n_0}}\frac{dN_{n_0}}{dt}\right]. \tag{50}$$

We can now combine with the other terms of Eq. (47) to obtain an expression which only depends on the rates of change of the conserved variables $(N_{n0}, \mathcal{N}'_n)$. Defining

$$\xi_{n'} = \frac{C_{v,n'}T_n^2}{\left(\overline{\Delta E'}_n + T_n^2\dfrac{d\ln\tilde{g}'_n}{dT_n}\right)} \quad\text{and}\quad \omega_{n'} = \xi_{n'}\frac{\mathcal{N}_{n'}}{N_{n_0}} \tag{51}$$

and adding the contribution from the ground state of the group, we obtain

$$\frac{d\mathcal{E}_n}{dt} = \left[E_{n_0} - \omega_{n'}\right]\frac{dN_{n_0}}{dt} + \left[E_{n_0} + \langle\Delta E\rangle_{n'} + \xi_{n'}\right]\frac{d\mathcal{N}'_n}{dt}. \tag{52}$$

One can then identify the rates of change of the population density with the effective rates. Considering transitions between groups n and $m > n$, and using a similar expression for $d\mathcal{E}_m/dt$, we have

$$\begin{aligned}\tilde{\alpha}^E_{(m_0|n_0)} &= \left[E_{m_0} - \omega_{m'} - E_{n_0} + \omega_{n'}\right]\cdot\tilde{\alpha}_{(m_0|n_0)}\\ &\equiv \bar{\varepsilon}_{(m_0|n_0)}\cdot\tilde{\alpha}_{(m_0|n_0)},\end{aligned} \tag{53a}$$

$$\begin{aligned}\tilde{\alpha}^E_{(m'|n_0)} &= \left[E_{m_0} + \langle\Delta E\rangle_{m'} + \xi_{m'} - E_{n_0} + \omega_{n'}\right]\cdot\tilde{\alpha}_{(m'|n_0)}\\ &\equiv \bar{\varepsilon}_{(m'|n_0)}\cdot\tilde{\alpha}_{(m'|n_0)},\end{aligned} \tag{53b}$$

$$\begin{aligned}\tilde{\alpha}^E_{(m_0|n')} &= \left[E_{m_0} - \omega_{m'} - E_{n_0} - \langle\Delta E\rangle_{n'} - \xi_{n'}\right]\cdot\tilde{\alpha}_{(m_0|n')}\\ &\equiv \bar{\varepsilon}_{(m_0|n')}\cdot\tilde{\alpha}_{(m_0|n')},\end{aligned} \tag{53c}$$

$$\begin{aligned}\tilde{\alpha}^E_{(m'|n')} &= \left[E_{m_0} + \langle\Delta E\rangle_{m'} + \xi_{m'} - E_{n_0} - \langle\Delta E\rangle_{n'} - \xi_{n'}\right]\cdot\tilde{\alpha}_{(m'|n')}\\ &\equiv \bar{\varepsilon}_{(m'|n')}\cdot\tilde{\alpha}_{(m'|n')}.\end{aligned} \tag{53d}$$

It is instructive to examine the limit of infinite Boltzmann temperatures; in this case,

$$\mathcal{Z}_{n'} \to g'_n, \quad C_{v,n'}, \xi_{n'}, \omega_{n'} \to 0 \quad\text{and}\quad \langle\Delta E\rangle_{n'} \to \overline{\Delta E'}_n$$

and similarly for m'. Equation (52) becomes

$$\frac{d\mathcal{E}_n}{dt} = E_{n_0}\frac{dN_{n_0}}{dt} + \frac{\sum_{i\in n'} g_i E_i}{g'_n}\frac{\mathcal{N}_{n'}}{dt} = E_{n_0}\frac{dN_{n_0}}{dt} + \frac{\sum_{i\in n'} g_i E_i}{g_{n_0}}\frac{dN_{n_0}}{dt}$$
$$= \frac{\sum_{i\in n} g_i E_i}{g_{n_0}}\frac{dN_{n_0}}{dt} = \tilde{E}_n\frac{d\mathcal{N}_n}{dt}, \tag{54}$$

where we have also used the fact that in that limit, $N_{n_0}/g_{n_0} = \mathcal{N}_n/g_n$, and used the definition of the average group energy—see Eq. (45). Since a similar equation is found for $d\mathcal{E}_m/dt$, the combination exactly yields Eq. (45). Thus, we have verified that by taking the limit $T_n, T_m \to \infty$, we recover the uniform group model.

For ionizations and recombinations, a similar procedure can be found. Considering the change in electron energy due to ionization and recombination from and to the group n, we have

$$\left.\frac{dE_e}{dt}\right)_n = -\sum_{i\in n}\frac{dN_i}{dt}I_i = -\frac{d}{dt}\left[\langle I\rangle_n \mathcal{N}_n\right]$$
$$= -I_{n_0}\frac{dN_{n_0}}{dt} - \langle I\rangle_{n'}\frac{d\mathcal{N}_{n'}}{dt} - \mathcal{N}_{n'}\frac{d\langle I\rangle_{n'}}{dt}, \tag{55}$$

where I_i is the ionization potential for level i and $\langle I\rangle_{n'}$ is the group ionization potential averaged over the sub-partition n'. Using $I_i = I_H - E_i = I_{n_0} - \Delta E_i$, it is easy to see that

$$\langle I\rangle_{n'} = I_{n_0} - \langle \Delta E\rangle_{n'} \quad \text{and} \quad \frac{d\langle I\rangle_{n'}}{dt} = -C_{v,n'}. \tag{56}$$

Equations (49) and (50) are still valid, and using again the definitions (51), we obtain the final form

$$\left.\frac{dE_e}{dt}\right)_n = -\left[I_{n_0} + \omega_{n'}\right]\frac{dN_{n_0}}{dt} - \left[I_{n_0} - \langle \Delta E\rangle_{n'} - \xi_{n'}\right]\frac{d\mathcal{N}_{n'}}{dt}. \tag{57}$$

Note the similarity with Eq. (52). The effective rates are therefore

$$\tilde{\alpha}^E_{(+|n_0)} = \left[I_{n_0} + \omega_{n'}\right]\cdot\tilde{\alpha}_{(+|n_0)} \equiv \bar{\varepsilon}_{(+|n_0)}\cdot\tilde{\alpha}_{(+|n_0)}, \tag{58a}$$

$$\tilde{\alpha}^E_{(+|n')} = \left[I_{n_0} - \langle \Delta E\rangle_{n'} - \xi_{n'}\right]\cdot\tilde{\alpha}_{(+|n')} \equiv \bar{\varepsilon}_{(+|n')}\cdot\tilde{\alpha}_{(+|n')}. \tag{58b}$$

Examination of equations (53) and (58) reveals that the overall procedure consists of replacing the energy of the group's ground state n_0 and sub-partition n' by *effective energies* for the energy exchange

$$\tilde{E}_{n_0} = E_{n_0} - \omega_{n'} \quad \text{and} \quad \tilde{E}_{n'} = E_{n_0} + \langle \Delta E\rangle_{n'} + \xi_{n'}. \tag{59}$$

Thus, the effective rates of energy transfer become

$$\tilde{\alpha}^E_{(m_0|n_0)} = \left(\tilde{E}_{m_0} - \tilde{E}_{n_0}\right)\cdot\tilde{\alpha}_{(m_0|n_0)}, \tag{60a}$$

$$\tilde{\alpha}^E_{(m'|n_0)} = \left(\tilde{E}_{m'} - \tilde{E}_{n_0}\right)\cdot\tilde{\alpha}_{(m'|n_0)}, \tag{60b}$$

$$\tilde{\alpha}^E_{(m_0|n')} = \left(\tilde{E}_{m_0} - \tilde{E}_{n'}\right)\cdot\tilde{\alpha}_{(m_0|n')}, \tag{60c}$$

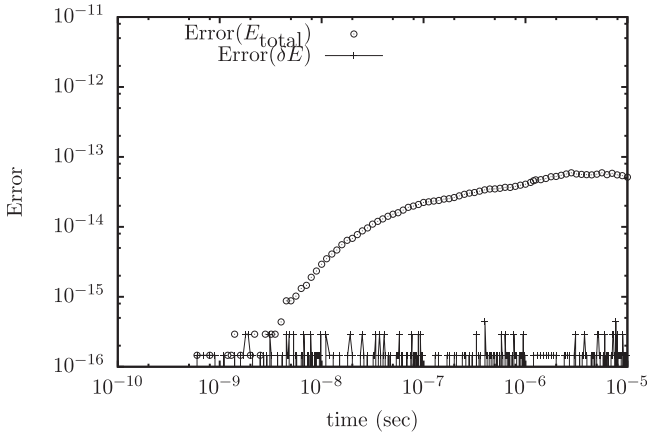

FIG. 14. Cumulative and instantaneous relative errors in energy conservation—test case 3—with revised formulation.

$$\tilde{\alpha}^E_{(m'|n')} = \left(\tilde{E}_{m'} - \tilde{E}_{n'}\right)\cdot\tilde{\alpha}_{(m'|n')} \tag{60d}$$

and for ionization:

$$\tilde{\alpha}^E_{(+|n_0)} = \left(I_H - \tilde{E}_{n_0}\right)\cdot\tilde{\alpha}_{(+|n_0)}, \tag{61a}$$

$$\tilde{\alpha}^E_{(+|n')} = \left(I_H - \tilde{E}_{n'}\right)\cdot\tilde{\alpha}_{(+|n')}. \tag{61b}$$

The use of effective group energies[36] provides a straightforward approach, and the effective rates of energy transfer for *all* transitions (including de-excitations, recombination, and radiative transitions) can now be expressed in a simple form. Note that Eq. (61) is similar to the case of uniform grouping (45) and since we have already demonstrated that we can recover the uniform grouping case in the limit of infinite temperatures, we have achieved here a fully consistent model.

We are now left with the task of verifying energy conservation with this revised approach. Using the same test case (3), we now find a much smaller level of error, as can be seen from Figure 14—compare with Figure 13—that is the characteristic of the level of numerical round-off. Note that the cumulative error sums the absolute values of the stepwise error (L_1 norm), and is therefore a maximum bound. Figure 15 shows the effect of bin size on the relative error;

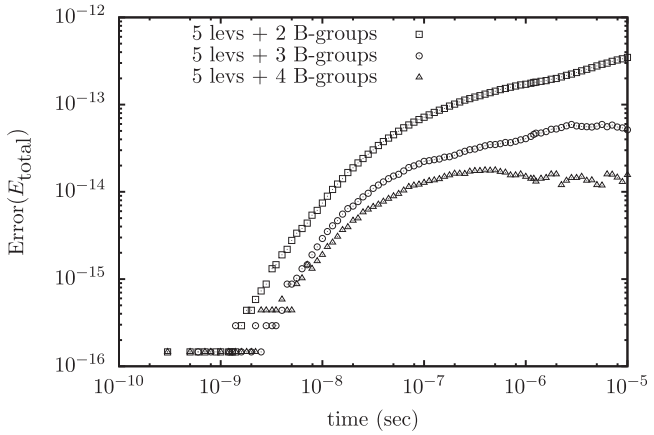

FIG. 15. Cumulative relative errors in energy conservation as function of group sizes; revised formulation.

this observation is similar to the one made regarding the accuracy of the ASDF—see Figure 5, i.e., smaller group widths are preferred. However, it is clear that even for one or two bins, the error on energy conservation remains very small.

VI. CONCLUDING REMARKS

In this paper, we described a model reduction mechanism for the collisional-radiative kinetics of the ASDF, by grouping electronic states into groups and deriving the corresponding macroscopic rates to take in account all the transitions. While level-grouping is a commonly used and necessary procedure when dealing with a very large number of atomic levels, as in high-temperature plasma,[37,38] the procedure is commonly based on uniform grouping (i.e., simple average over the level degeneracies). A higher-order description of the internal structure of the groups was developed here by assuming a Boltzmann distribution of the levels within the group, with different temperatures for each group. This approach was shown here to have superior features to the uniform grouping procedure, as summarized below.

Numerical instabilities in the limit of low internal temperature led us to the design of this non-traditional approach. Instead of conserving the total energy of a group, we used a novel approach using conserved variables from a sub-partitioning of the group between the lowest level of that group (N_{n_0}) and the remaining states ($\mathcal{N}'_n$). Combined with an appropriate expansion of the sub-group partition function, this model was able to very rapidly determine the group temperatures in a stable and accurate fashion for all conditions, solving a problem that is particularly vexing for atomic collisional-radiative kinetics, due to the structure of the energy levels of atomic plasma.

The two grouping schemes (uniform and Boltzmann) were implemented on an electronic collisional-radiative model for atomic hydrogen and the results were compared with the full solution of the master equation on a large number of numerical tests, of which a representative sub-set was shown here. Both schemes showed agreement with the solution of the master equations and have excellent convergence properties. However, substantial accuracy improvements were obtained at minimal computational cost with the Boltzmann grouping. Detailed tests of energy conservation revealed the need for a revised approach to the construction of effective rates of energy transfer. This was made necessary because the total group energy was not part of the set of conserved variables, and consistency requirements led us to a new formulation involving effective level energies and average group energies between which energy exchange occurs. We derived this new formulation and showed that it was simple to implement, and consistent with the uniform grouping method.

For the case of atomic hydrogen studied here, it was sufficient to mix a few low-lying states with two Boltzmann groups for all the high energy states and be able to capture the correct ionization kinetics for all the states and the radiative spectrum. This significantly reduces the computational cost associated with solving the kinetics and therefore can be applied in multidimensional and time-resolved flow calculations, with accurate coupling to radiative processes. The reduction schemes presented in this work could also be applied to other set of kinetics, e.g., rovibrational collisional and vibrational kinetics, although in this case the levels are distributed much more uniformly on the energy axis, in which case reduction schemes and group temperature determination are more straightforward. Future work includes a straightforward extension of the approach to non-hydrogenic and multi-stage ionization, as well as the application of more accurate and more efficient time integration schemes, currently under development. Further optimization of the scheme, such as dynamic re-partitioning, is also under exploration.

ACKNOWLEDGMENTS

We wish to acknowledge the support of the Air Force Office of Scientific Research (AFOSR), Grant No. 12RZ06COR (PM: Dr. F. Fahroo) for this work.

APPENDIX: COMPUTATION OF KINETIC RATES

The classical form of the cross-section for energy exchange between a free electron and the atom,[6] leading to an excitation from level n to level $m > n$ is

$$\sigma^e_{nm} = (4\pi a_0^2)\frac{I_H^2(\varepsilon - E_{nm})}{E_{nm}\varepsilon^2}\cdot(3\mathrm{f}_{nm}), \tag{A1}$$

where a_0 is the Bohr radius, ε is the energy of the free electron, $\Delta E_{nm} = E_m - E_n$ is the energy gap between n and m and f_{nm} is the oscillator strength

$$\mathrm{f}_{nm} = \frac{32}{3\pi\sqrt{3}}\frac{1}{n^5}\frac{1}{m^3}\frac{1}{\left(\frac{1}{n^2}-\frac{1}{m^2}\right)^3}. \tag{A2}$$

The free electrons are assumed to follow an isotropic Maxwellian distribution $f_e(\varepsilon_e)$

$$f_e(\varepsilon_e)d\varepsilon_e = \frac{2}{\sqrt{\pi}(kT_e)^{3/2}}\varepsilon_e^{1/2}e^{-\varepsilon_e/kT_e}d\varepsilon_e, \tag{A3}$$

where m_e is the electron mass, $\varepsilon_e = m_e v_e^2/2$ and T_e is the temperature. The rate of excitation is obtained by averaging over the distribution function

$$\alpha^e_{(m|n)} = \int_{E_{nm}}^{\infty}\sigma^e_{nm}(\varepsilon)v_e f(v_e)dv_e, \tag{A4}$$

leading to

$$\alpha^e_{(m|n)} = (4\pi a_0^2)\bar{v}_e\left(\frac{I_H}{kT_e}\right)^2(3\mathrm{f}_{nm})\psi_{nm}, \tag{A5}$$

where

$$\bar{v}_e = \left(\frac{8kT_e}{\pi m_e}\right)^{\frac{1}{2}}, \quad \psi_{nm} = \frac{e^{-x_{nm}}}{x_{nm}} - E_1(x_{nm}), \quad \text{and}$$
$$E_1(x) = \int_x^\infty \frac{e^{-y}}{y} dy. \tag{A6}$$

Here, $\bar{v}_e$ is the mean thermal electron velocity, $x_{nm} = \Delta E_{nm}/kT_e$ and E_1 is the exponential integral. The reverse rate can be found from detailed balance

$$\beta^e_{(n|m)} = \frac{n^2}{m^2} e^{+x_{nm}} \cdot \alpha_{(m|n)}. \tag{A7}$$

We use the low temperature approximation[6] ($x_{nm} \gg 1$)

$$E_1(x) \simeq \frac{e^{-x}}{x}\left(1 - \frac{1}{x}\right), \tag{A8}$$

in which case

$$\alpha^e_{(m|n)} \simeq \left[4\pi a_0^2 \cdot \frac{32}{\pi\sqrt{3}} \cdot \bar{v}_e\right] \frac{e^{-x_{nm}}}{n^5 m^3 (n^{-2} - m^{-2})^5}, \tag{A9a}$$

$$\beta^e_{(n|m)} \simeq \left[4\pi a_0^2 \cdot \frac{32}{\pi\sqrt{3}} \cdot \bar{v}_e\right] \frac{1}{n^3 m^5 (n^{-2} - m^{-2})^5}. \tag{A9b}$$

The factor in brackets is an upper bound, which is reached for the upper states when $x_{nm} \to 0$. Another scale is the factor I_H/kT_e in x_{nm}, which is effectively responsible for the stiffness. If that factor is very low (high temperatures), all rates are of the same order; at low temperatures, the exponential term dominates and the range of time scales is increased.

The cross-section for ionization by electron impact has a form similar to Eq. (A1), i.e.,

$$\sigma^e_n = (4\pi a_0^2) \frac{I_H^2(\varepsilon - I_n)}{I_n \varepsilon^2}. \tag{A10}$$

This leads to an ionization rate coefficient[6]

$$\alpha^e_{(+|n)} = (4\pi a_0^2)\bar{v}_e \left(\frac{I_H}{kT_e}\right)^2 \psi(x_n). \tag{A11}$$

The final state $(+|$ is an ionized state, i.e., where one electron initially bound to the atom has reached the ionization limit ($n = \infty$) and is part of a free continuum of states. Using the principle of detailed balance, the reverse (recombination) rate is

$$\beta^e_{(n|+)} \simeq \left[\frac{4}{\pi}\frac{a_0^2 h^3}{m_e^2 kT_e}\right] \left(\frac{I_H}{kT_e}\right)^2 n^2 \psi(x_n) e^{x_n}. \tag{A12}$$

Using the same low temperature approximation (A8), we obtain[6]

$$\alpha^e_{(+|n)} \simeq (4\pi a_0^2)\left(\frac{8kT_e}{\pi m_e}\right)^{1/2} n^4 e^{-x_n}, \tag{A13a}$$

$$\beta^e_{(n|+)} \simeq \left[\frac{4}{\pi}\frac{a_0^2 h^3}{m_e^2 kT_e}\right] n^6. \tag{A13b}$$

The rates of radiative transitions between levels can also be obtained classically for the hydrogen atom.[5] The spontaneous emission rates from an upper level m are

$$A_{(n|m)} = \left(\frac{8\pi^2 e^2}{m_e c^3}\right)\frac{g_n}{g_m} \mathrm{f}_{nm} = \frac{1.6 \times 10^{10}}{m^3 n(m^2 - n^2)} \mathrm{s}^{-1}. \tag{A14}$$

The expression on the right is for atomic hydrogen only.

[1] R. G. Jahn, *Physics of Electric Propulsion* (Dover Publications, 2006).
[2] M. Capitelli, C. M. Ferreira, B. F. Gordiets, and A. I. Osipov, *Plasma Kinetics in Atmospheric Gases* (Springer, 2000).
[3] I. H. Hutchinson, *Principles of Plasma Diagnostics*, 2nd ed. (Cambridge University Press, 2005).
[4] W. G. Vincenti and C. H. Kruger, *Introduction to Physical Gas Dynamics* (Krieger Pub Co, 1975).
[5] M. Mitchner and C. H. Kruger, *Partially Ionized Gases*, 1st ed. (John Wiley and Sons, 1973).
[6] Y. B. Zel'dovich and Y. P. Raizer, *Physics of Shock Waves and High Temperature Hydrodynamic Phenomena*, 3rd ed. (Dover Publication, 2002).
[7] I. Armenise, M. Capitelli, R. Celiberto, G. Colonna, C. Gorse, and A. Lagani, "The effect of $N + N_2$ collisions on the non-equilibrium vibrational distributions of nitrogen under reentry conditions," Chem. Phys. Lett. **227**, 157–163 (1994).
[8] A. Bultel, B. G. Cheron, A. Bourdon, O. Motapon, and I. F. Schneider, "Collisional-radiative model in air for earth re-entry problems," Phys. Plasmas **13**, 043502 (2006).
[9] C. O. Laux, L. Pierrot, and R. J. Gessman, "State-to-state modeling of a recombining nitrogen plasma experiment," Chem. Phys. **398**, 46–55 (2012).
[10] M. G. Kapper and J.-L. Cambier, "Ionizing shocks in argon. Part I: Collisional-radiative model and steady-state structure," J. Appl. Phys. **109**, 113308 (2011).
[11] M. G. Kapper and J.-L. Cambier, "Ionizing shocks in argon. Part II: Transient and multi-dimensional effects," J. Appl. Phys. **109**, 113309 (2011).
[12] M. Panesi, T. Magin, A. Bourdon, A. Bultel, and O. Chazot, "Electronic excitation of atoms and molecules for the FIRE II flight experiment," J. Thermophys. Heat Transfer **25**, 361–374 (2011).
[13] M. Panesi, R. L. Jaffe, D. W. Schwenke, and T. E. Magin, "Rovibrational internal energy transfer and dissociation of N2(1Σg+)-N(4S(u)) system in hypersonic flows," J. Chem. Phys. **138**, 044312 (2013).
[14] E. Josyula and W. Bailey, "Vibration-dissociation coupling using master equations in nonequilibrium hypersonic blunt-body flow," J. Thermophys. Heat Transfer **15**, 157–167 (2001).
[15] D. Giordano, V. Bellucci, G. Colonna, M. Capitelli, I. Armenise, and C. Bruno, "Vibrationally relaxing flow of N2 past an infinite cylinder," J. Thermophys. Heat Transfer **11**, 27–35 (1997).
[16] G. Colonna, L. Pietanza, and M. Capitelli, "Recombination-assisted nitrogen dissociation rates under nonequilibrium conditions," J. Thermophys. Heat Transfer **22**, 399–406 (2008).
[17] T. E. Magin, M. Panesi, A. Bourdon, R. L. Jaffe, and D. W. Schwenke, "Coarse-grain model for internal energy excitation and dissociation of molecular nitrogen," Chem. Phys. **398**, 90–95 (2012).
[18] A. Guy, A. Bourdon, and M.-Y. Perrin, "Consistent multi-internal-temperatures models for nonequilibrium nozzle flows," Chem. Phys. **420**, 15–24 (2013).
[19] Y. Liu, M. Vinokur, M. Panesi, and T. Magin, "A multi-group maximum entropy model for thermo-chemical non-equilibrium," AIAA Paper 2010-4332, 2010.
[20] J. Vlcek, "A collisional-radiative model applicable to argon discharges over a wide range of conditions. I. Formulation and basic data," J. Phys. D: Appl. Phys. **22**, 623 (2000).
[21] Two of the test cases considered here are isothermal, i.e., T_e = constant. The third test case has a variable T_e but is designed only to test energy conservation, and hence radiative energy losses would not serve this purpose.

[22]Strictly speaking, the ionization limit I_H is attained for $n \to \infty$. In reality, the ionization potential is lowered as a result of interaction with the plasma (Debye shielding) and quantum uncertainty. In practice, the truncation is accomplished at a lower limit still; for the current purpose, details of this truncation procedure can be ignored. Suffice to say that the series extends to a number $n = M$, which can be considered large, e.g., O(100).

[23]That is, within the group.

[24]For further ease of notation, the Boltzmann constant k is not explicitly written.

[25]T. Magin, M. Panesi, A. Bourdon, R. Jaffe, and D. Schwenke, "Rovibrational internal energy excitation and dissociation of molecular nitrogen in hypersonic flows," AIAA Paper 2010-4336, 2010.

[26]In a log-plot, this model assumes that the slope within each "bin" is always the same, and is not related to the average slope determined by the difference between adjacent bins.

[27]Note that this problem is particularly relevant to ASDF kinetics because of the geometric progression of the energy levels. By performing tests on a pseudo-atom with equidistant energy levels, stability of the iterations was much improved, although not entirely eliminated for some conditions.

[28]We have here temporarily simplified the notation ($g_0 \equiv g_{n_0}$, $g_1 \equiv g_{n_0+1}$, …).

[29]This approach is a reflection of the self-similar structure of the atomic levels.

[30]Since we are considering electron collisions only, all test cases must start with an initial degree of ionization $x_e \neq 0$.

[31]This understandably so, since the ladder-climbing process of the early evolution would be difficult to describe with grouping methods, even by 1st-order approximation of the internal distribution within the groups.

[32]By coincidence, the results of uniform binning for 6 resolved levels is right on top of the solution for a Boltzmann group with 4 lower levels.

[33]Although the grouping techniques are formulated here for a general set of kinetics, the effectiveness of the grouping approach is problem specific. For other situations, e.g., ro-vibrational states, a different strategy may be required than the one discussed here for atomic states.

[34]J.-L. Cambier and S. Moreau, "Simulations of a molecular plasma in collisional-radiative nonequilibrium," AIAA Paper No. 93-3196; 24th AIAA Plasma Dynamics Conference, Orlando, FL, 1993.

[35]Note that the scheme includes numerical errors resulting from the forward and backward sweeps of the Gaussian elimination procedure. However, this is negligible here, since we have used double-precision.

[36]Contrary to the uniform grouping case, we need to use two values, one for n_0 and one for n', which reflects the additional degrees of freedom in the Boltzmann model.

[37]H. A. Scott and S. B. Hansen, "Advances in NLTE modeling for integrated simulations," High Energy Density Phys. **6**, 39–47 (2010).

[38]S. B. Hansen, J. Bauche, and C. Bauche-Arnoult, "Superconfiguration widths and their effects on atomic models," High Energy Density Phys. **7**, 27–37 (2011).